Mechanisms for High Displacement Efficiency of Low-Temperature CO_2 Floods

R. Okuno, SPE, University of Alberta; **R.T. Johns,** SPE, Pennsylvania State University; and **K. Sepehrnoori,** SPE, University of Texas at Austin

Summary

CO_2 floods at temperatures typically below 120°F can involve complex phase behavior, where a third CO_2-rich liquid (L_2) phase coexists with the oleic (L_1) and gaseous (V) phases. Results of slim-tube measurements in the literature show that an oil displacement by CO_2 can achieve high displacement efficiency of more than 90% when three hydrocarbon phases coexist during the displacement. However, the mechanism for the high-displacement efficiency is uncertain because the complex interaction of phase behavior with flow during the displacement is not fully understood.

In this paper, we present the first detailed study of three-phase behavior predictions and displacement efficiency for low-temperature CO_2 floods. Four-component EOS models are initially used to investigate systematically the effects of pressure, temperature, and oil properties on development of three-phase regions and displacement efficiency. Multicomponent oil displacements by CO_2 are then considered. We use a compositional reservoir simulator capable of robust three-phase equilibrium calculations.

Results show that high displacement efficiency of low-temperature CO_2 floods is a consequence of both condensing and vaporizing behavior. The L_2 phase serves as a buffer between the immiscible V and L_1 phases within the three-phase region. Components in the L_1 phase first transfer efficiently to the L_2 phase near a lower critical endpoint (LCEP). These oil components then transfer to the V phase near an upper critical endpoint (UCEP) at the trailing edge of the three-phase region. The CEPs are defined where two of the three coexisting phases merge in the presence of the other immiscible phase. Unlike two-phase displacements, condensation and vaporization of intermediate components occur simultaneously within the three-phase region. The simultaneous condensing/vaporizing behavior involving the CEPs is also confirmed for simulations of several west Texas oil displacements. Quaternary fluid models can predict qualitatively the complex displacements because four is the minimum number of components to develop CEP behavior in composition space at a fixed temperature and pressure.

Introduction

Mixtures of reservoir oil and CO_2 can exhibit complex phase behavior at temperatures typically below 120°F, where the L_2 phase can coexist with the L_1 and V phases (Huang and Tracht 1974; Shelton and Yarborough 1977; Metcalfe and Yarborough 1979; Gardner et al. 1981; Henry and Metcalfe 1983; Orr and Jensen 1984; Turek et al. 1988; Khan et al. 1992; Creek and Sheffield 1993). Slim-tube measurements reported in the literature show that low-temperature oil displacements by CO_2 involving three hydrocarbon phases can achieve high displacement efficiency of more than 90% (Yellig and Metcalfe 1980; Gardner et al. 1981; Orr et al. 1981, 1983; Henry and Metcalfe 1983; Khan 1992; Creek and Sheffield 1993).

Several correlations for two-phase minimum miscibility pressures (MMPs) for CO_2 floods have been proposed. In Holm and Josendal (1974), reservoir temperature and molecular weight for C_{5+} in the oil are the correlation parameters. Yellig and Metcalfe (1980) used reservoir temperature as the correlation parameter for MMP and assumed that the MMP was independent of oil composition. Both correlations can appreciably be in error, especially for three-hydrocarbon phases (Stalkup 1978; Holm and Josendal 1980; Yuan et al. 2005). Orr and Jensen (1984) proposed to use the vapor pressure of CO_2 (extrapolated if necessary) as a rough estimate of the CO_2 MMP for low-temperature oil reservoirs. Their correlation is based on experimental results indicating that an L_2 phase extracts hydrocarbons efficiently and appears as a L_1-L_2-V region on a P–x diagram at pressures near the vapor pressure of CO_2. Creek and Sheffield (1993) observed in their experiments that the measured CO_2-MMPs for Permian Basin oils always coincide with the lower boundary of the L_1-L_2-V regions on the P–x diagrams.

The correlation of Orr and Jensen (1984) and the observations of Creek and Sheffield (1993) indicate that existence of a three-phase region plays an important role for high efficiency of low-temperature oil displacements by CO_2. Measured CO_2 MMPs reported in the literature typically fall in a pressure range where three hydrocarbon phases coexist during a displacement. However, it is unknown whether or not the thermodynamic MMP is achieved within such a pressure range. The thermodynamic MMP is defined as the minimum displacement pressure at which complete miscibility is developed along the composition path from injection gas to the reservoir oil for 1D flow in the absence of dispersion.

Gas-injection theory for oil displacements involving only L-V equilibrium shows that miscibility is developed at a two-phase critical point even when a composition path goes through a two-phase region (Johns and Orr 1996; Orr 2007). That is, existence of two-phase immiscible flow in the presence of dispersion does not necessarily mean a partially miscible (or immiscible) displacement. LaForce (2005) and LaForce and Johns (2005) studied analytical composition paths for displacements exhibiting three-phase immiscibility using ternary mixtures. They concluded that a composition path that goes through a three-phase region cannot develop multicontact miscibility. Thus, development of complete miscibility has not been proven for displacements exhibiting three-phase flow.

A question then arises as to why low-temperature oil displacements by CO_2 can achieve high displacement efficiency in spite of the three-hydrocarbon-phase flow. Several authors attempted to explain why low-temperature oil displacements by CO_2 can achieve high displacement efficiency. The most common explanation is that an L_2 phase can efficiently extract a certain range of hydrocarbons in the reservoir oil [i.e., selectivity of a liquid CO_2 phase (Huie 1972)]. Creek and Sheffield (1993) stated that Permian Basin oil displacements by CO_2 resulted in high displacement efficiencies because of efficient extraction of midrange hydrocarbons into an L_2 phase. Holm and Josendal (1974, 1982) reported that a CO_2-rich vapor phase extracts carbon numbers up to C_6, and an L_2 phase can extract components as heavy as C_{30}. They concluded that the CO_2 MMP is inversely proportional to the amount of extractable hydrocarbons (i.e., C_5–C_{30} in their papers) present in the reservoir oil. Stewart and Nielsen (1953) reported that light components are extracted into an L_2 phase more than heavy components. Turek et al. (1988) reported that an L_2 phase can extract a significant portion of all but the heaviest hydrocarbon components in the reservoir oil. Orr et al. (1981) stated that an L_2 phase can extract components as heavy as C_{24}, while Gardner et al. (1981) stated that it can extract hydrocarbons heavier than C_{35}. Orr et al. (1983) reported that an L_2 phase can contain 30% by weight hydrocarbons, and that a

Copyright © 2011 Society of Petroleum Engineers

This paper (SPE 129846) was accepted for presentation at the SPE Symposium on Improved Oil Recovery, Tulsa, 24–28 April 2010, and revised for publication. Original manuscript received for review 27 June 2010. Revised manuscript received for review 22 November 2010. Paper peer approved 27 January 2011.

Downloaded from http://onepetro.org/SJ/article-pdf/16/04/751/2106980/spe-129846-pa.pdf/1 by The University of Texas At Austin user on 18 September 2022

CO_2-rich vapor phase at the same temperature and pressure extracts hydrocarbons less efficiently.

Orr et al. (1981, 1983) and Gardner et al. (1981) simulated their slim-tube experiments for CO_2/low-temperature-oil systems using a simplified finite-difference simulator. In their simulations, phase behavior predictions were based on polynomial representations for the pseudoternary diagrams [e.g., CO_2, C_{1-6}, and C_{7+} in Gardner et al. (1981)] obtained from their single- and multicontact experiments. Their three-phase region (tie triangle) was invariant because there are zero degrees of freedom in a ternary diagram at a fixed temperature and pressure. The equilibrium compositions of their tie triangle were not directly measured, but estimated based on neighboring two-phase regions. From their ternary simulations, Orr et al. (1981, 1983) and Gardner et al. (1981) concluded that significant extraction of hydrocarbons by the L_2 phase accounts for the observed high displacement efficiency for CO_2/low-temperature-oil systems. However, their results are likely not representative of displacements of multicomponent oils where the equilibrium compositions of tie triangles are not invariant. This likely explains the deviations of oil-recovery predictions from experimental results for three-hydrocarbon-phase displacements in Orr et al. (1983).

The common explanation based on the extraction of oil components by an L_2 phase cannot predict under what conditions the extraction becomes efficient. Extraction of oil components by an L_2 phase depends on thermodynamic conditions such as temperature, pressure, and composition. We show in this paper that the actual phase behavior encountered during a displacement is more involved than the simple extraction described only by the L_2 phase.

Understanding L_1-L_2-V displacements requires knowledge of complex mass transfer among the three phases. However, details of three-phase behavior during low-temperature CO_2 flooding are relatively unknown. This is primarily because such phase behavior is conventionally presented using a pressure-composition (P–x) diagram, which presents phase behavior along the mixing line between the oil and injection gas, instead of the actual composition path observed during a displacement. A second reason is that most compositional simulators are not capable of robust three-phase equilibrium calculations. A third reason is because prior research used pseudoternary diagrams to study the effect of three-phase behavior on displacement efficiency. Ternary systems cannot model complex three-phase behavior because a three-phase region is invariant on a ternary diagram.

There are two main objectives in this paper. The first is to explain the mechanism for high efficiency of displacements involving complex three-hydrocarbon-phase behavior. The second is to understand complex three-phase behavior during low-temperature oil displacements by CO_2. To simulate three-phase behavior during oil displacements, we use UTCOMP (Chang et al. 1990), which has been updated with the robust and fast phase equilibrium algorithms developed by Okuno (2009) and Okuno et al. (2010a, b, c). Oil/CO_2-solvent mixtures are modeled initially using quaternary fluid models with the Peng-Robinson EOS (Peng and Robinson 1976). We investigate systematically the mechanism for high efficiency of low-temperature CO_2 floods with varying pressure, temperature, and oil properties. Then, the mechanism identified is confirmed with displacement simulations of a west Texas oil using seven components.

Investigation of Three-Phase Behavior and Its Effect on Displacement Efficiency

The purpose of this section is to identify the mechanism for high displacement efficiency of low-temperature CO_2 floods. Using quaternary displacements, we systematically investigate the complex three-hydrocarbon-phase behavior and its effect on displacement efficiency at different pressures, temperatures, and oil-component properties.

Method for Systematic Investigation. Phase behavior of a fluid consisting of N_C components can be mathematically considered as a function that spans (N_C + 1) dimensions [i.e., temperature, pressure, and (N_C − 1) component mole fractions]. Because of the high dimension, the phase behavior of solvent/reservoir-oil mixtures is conventionally presented using a pseudobinary P–x diagram. However, such a P–x diagram does not fully describe the thermodynamic space for analyzing gas injection because it is a cross section of the phase behavior only along the mixing line between the two pseudocomponents (i.e., oil and gas).

Orr et al. (1981, 1983) and Gardner et al. (1981) used ternary diagrams to model three-phase behavior of CO_2/low-temperature-oil mixtures and studied the effect of the L_2 phase on the displacement efficiency. They concluded that ternary representation can be used to model low-temperature oil displacements by CO_2. However, a three-phase region has no degrees of freedom in a ternary diagram, and compositions of the three equilibrium phases cannot vary, unlike those in real oil displacements.

We use four components to allow for CEP behavior in composition space at a fixed temperature and pressure. A CEP is defined where two of the three coexisting phases merge in the presence of the other immiscible phase (e.g., Uzunov 1993). There are two types of CEP behavior for mixtures of CO_2 and hydrocarbons. The first CEP is where the L_1 and L_2 phases merge in the presence of the V phase ($L_1 = L_2$–V). The other CEP is where the L_2 and V phases merge in the presence of the L_1 phase (L_1–$L_2 = V$). The phase rule for critical points predicts that four is the minimum number of components to develop CEP behavior at a fixed temperature and pressure [see Okuno (2009)].

For binary three-phase behavior, the CEP of type $L_1 = L_2$–V occurs at the low-temperature end of the three-phase curve in P–T–x space. The CEP of type L_1–$L_2 = V$ occurs at the high-temperature end of the three-phase curve in P–T–x space. Therefore, the phase behaviors $L_1 = L_2$–V and L_1–$L_2 = V$ are referred to as the lower critical endpoint (LCEP) and the upper critical endpoint (UCEP), respectively.

Three-phase behavior bounded by the two types of CEPs is observed in binary phase behavior types IV and V according to the classification of van Konynenburg (1968), Scott and van Konynenburg (1970), and van Konynenburg and Scott (1980). It is also observed for hydrocarbon mixtures (Rowlinson and Freeman 1961; Davenport and Rowlinson 1963; Davenport et al. 1966; Kohn et al. 1966; Wagner et al. 1968) and CO_2/n-C_{13} mixtures (Enick et al. 1985; Galindo and Blas 2002). All of these observations were made in static experiments, not in oil displacements by solvents. To the best of our knowledge, no research has reported an oil displacement that exhibits phase behavior characterized by a three-phase region bounded by the two CEPs, $L_1 = L_2$–V and L_1–$L_2 = V$. We consider CEP behavior because we found that it is the key to high displacement efficiency of low-temperature CO_2 floods, as will be presented in this paper.

Considering the Gibbs phase rule, a three-phase region has one degree of freedom at a given temperature and pressure for four components. That is, a three-phase region is a volumetric region in a quaternary diagram, as shown in **Fig. 1.** The three-phase region consists of an infinite number of tie triangles. A tie triangle changes its shape and size within the three-phase region. Two tie triangles are shown in Fig. 1 to illustrate tie triangles exhibiting near-CEP behavior. A CEP is not a point in composition space, but is a tie line where two of the three phases are critical in the presence of the other noncritical phase. From this point on, a CEP is called a CEP tie line to avoid the confusion.

We use the Peng-Robinson EOS to model three-phase behavior of CO_2/hydrocarbon mixtures. Use of an EOS provides a purely theoretical investigation, and it does not necessarily lead to quantitatively correct predictions. However, the qualitative trend should be correct considering the pioneering research on phase behavior predictions using the van der Waals EOS by van Konynenburg (1968), Scott and van Konynenburg (1970), and van Konynenburg and Scott (1980). Even one of the simplest cubic EOSs, the van der Waals EOS, never yields physically absurd predictions (van Konynenburg 1968). Various authors later confirmed that other cubic EOSs are also able to predict three-phase behavior at least qualitatively [e.g., Deiters and Schneider (1976), Chaback and Turek (1986), and Deiters and Pegg (1989) for the Redlich-Kwong EOS; Mushrif (2004), Yang (2006), Mushrif and Phoenix (2008), Gauter (1999), Gauter et al. (1999), Larson et al. (1989),

Downloaded from http://onepetro.org/SJ/article-pdf/16/04/751/2106980/spe-129846-pa.pdf/1 by The University of Texas At Austin user on 18 September 2022

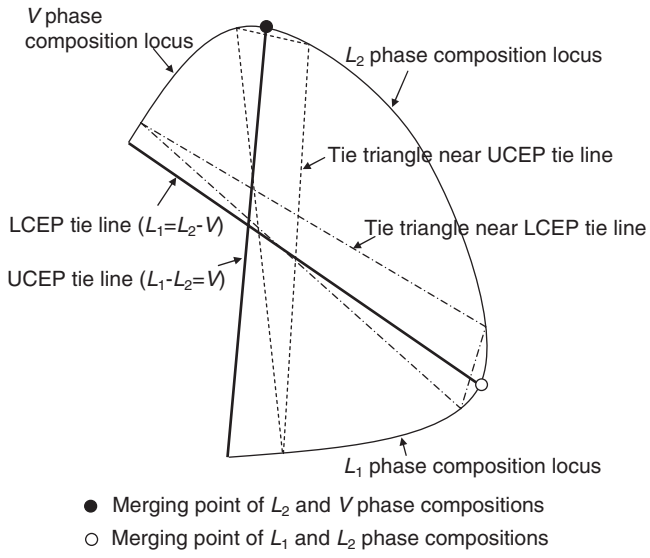

Fig. 1—Schematic of a three-phase region bounded by CEP tie lines for a quaternary system at a fixed temperature and pressure.

Khan et al. (1992), and Creek and Sheffield (1993) for the Peng-Robinson EOS; and Gregorowicz and de Loos (1996) and Coutinho et al. (1995) for the Soave-Redlich-Kwong EOS]. Khan et al. (1992) used the Peng-Robinson EOS fluid models for west Texas oils in their multiphase compositional simulations using UTCOMP. They successfully matched the slim-tube experimental data with their simulation results.

We make a four-component EOS fluid model based on the Bob Slaughter Block (BSB) oil (105°F) that was modeled by Khan et al. (1992) using seven components **(Table 1).** Three pseudocomponents C_{2-3}, C_{4-6}, and C_{7-15}, are grouped into one pseudocomponent C_{H1} for our four-component model. Two pseudocomponents, C_{16-27} and C_{28+}, are grouped into C_{H2}. This four-component (quaternary or Q) model for the BSB oil is referred to as the BSB-Q oil. The EOS parameters for the BSB-Q oil are given in **Table 2.** The critical temperatures and pressures for C_{H1} and C_{H2} are adjusted to match the oil density from the seven-component model within a pressure range from 14.7 to 2,500 psia, which contains the pressures of interest in our example displacements. Similarly, the critical volumes for C_{H1} and C_{H2} are adjusted to match the oil viscosity. The binary interaction coefficients (BICs) for C_{H1} and C_{H2} are calculated based on the mole fraction weighted average of BICs for the member components.

The BSB-Q oil model is not adjusted to match the phase diagrams and oil recoveries from the BSB oil model. Our main purpose in developing the BSB-Q oil is to study qualitatively the displacement mechanism of low-temperature CO_2 floods using the Peng-Robinson EOS.

The *P-x* diagram across the four-component phase behavior space for the pseudobinary mixture of the BSB-Q oil and injection gas given in Table 2 is shown in **Fig. 2.** The three-phase region exists in a pressure range between 1,190 and 1,485 psia at solvent mole fractions from 63 to 97%. Fig. 2 also shows a projection of the *P–T–x* diagram onto a *P–T* diagram for the pseudobinary mixture of the BSB-Q oil and injection gas. The three-phase equilibrium occurs near the binodal curve of the injection gas. The critical locus of $L = V$ critical points gradually changes its behavior to $L_1 = L_2$. This continuous transition can be observed for binary systems CO_2+*n*-alkane from *n*-C_{14} through *n*-C_{21} [e.g., Alwani and Schneider (1976) and Miller and Luks (1989)].

In subsequent subsections, the BSB-Q oil is considered as the base oil. First, we examine pressure effects on three-phase behavior in the BSB-Q composition space and on the efficiency of the BSB-Q oil displacements. We then change the properties of the BSB-Q oil by varying the properties of the heavy components C_{H1} and C_{H2}. Those new oils are compared with the BSB-Q oil in terms of three-phase behavior and displacement efficiency to see the effect of oil component properties. Last, temperature effects on three-phase behavior and oil displacements are studied.

Table 3 summarizes reservoir properties for simulations of the 1D oil displacements with no gravity. Those reservoir properties are used for all simulations in this paper. The aqueous phase exists at its residual saturation, so it does not flow. We perform a series of 1D simulations at different pressures. The injection and production wells are operated at constant bottomhole pressures. The pressure difference along the reservoir is set to 10 psi for all simulations

TABLE 1—FLUID PROPERTIES FOR SIMULATIONS FOR BOB SLAUGHTER BLOCK OIL (KHAN ET AL. 1992)

	Oil (Mol %)	Gas (Mol %)	Molecular Weight	T_C (°F)	P_C (psia)	Acentric Factor	V_C (ft³/lb-mol)	h	g	BIC* CO_2
CO_2	3.37	95.0	44.01	87.89	1069.87	0.225	1.51	1.0	1.000	0.000
C_1	8.61	5.0	16.04	–171.67	667.20	0.008	1.59	0.0	0.055	0.055
C_{2-3}	15.03	0.0	37.20	159.90	652.56	0.131	2.90	0.0	0.055	0.055
C_{4-6}	16.71	0.0	69.50	374.13	493.07	0.240	4.91	0.0	0.055	0.055
C_{7-15}	33.04	0.0	140.96	630.68	315.44	0.618	9.00	0.0	0.105	0.105
C_{16-27}	16.11	0.0	280.99	892.16	239.90	0.957	17.1	0.0	0.105	0.105
C_{28+}	7.13	0.0	519.62	1236.79	238.12	1.268	32.5	0.0	0.105	0.105

*All others are 0.0.

TABLE 2—FLUID PROPERTIES FOR BSB-Q OIL (A PSEUDOQUATERNARY MODEL FOR THE BSB OIL)

	Oil (Mol %)	Gas (Mol %)	Molecular Weight	T_C (°F)	P_C (psia)	Acentric Factor	V_C (ft³/lb-mol)	h	g	BIC* CO_2
CO_2	3.37	95.0	44.01	87.89	1069.87	0.225	1.51	1.0	1.000	0.000
C_1	8.61	5.0	16.04	–171.67	667.20	0.008	1.59	0.0	0.055	0.055
C_{H1}	64.78	0.0	98.45	492.58	396.21	0.481	6.60	0.0	0.081	0.081
C_{H2}	23.24	0.0	354.20	971.92	251.05	1.042	20.55	0.0	0.105	0.105

*All others are 0.0.

Downloaded from http://onepetro.org/SJ/article-pdf/16/04/751/2106980/spe-129846-pa.pdf/1 by The University of Texas At Austin user on 18 September 2022

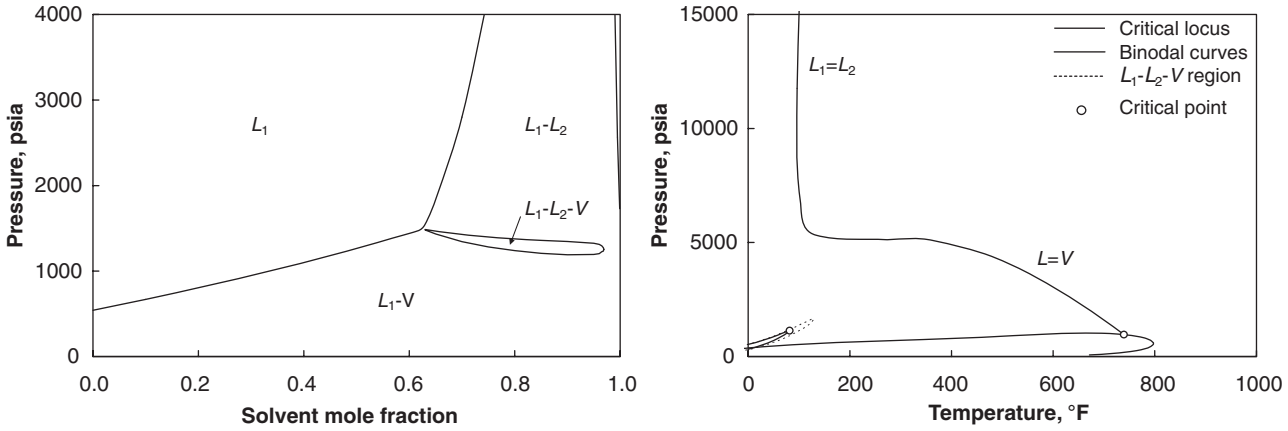

Fig. 2—Phase diagrams for the pseudobinary mixture of the BSB-Q oil and injection gas given in Table 2. Left: *P–x* diagram at 105°F. Right: *P–T* projection of the *P–T–x* diagram.

TABLE 3—RESERVOIR PROPERTIES FOR SIMULATIONS OF 1D OIL DISPLACEMENTS

			Corey			
Dimensions	1000 ft × 10 ft × 10 ft	Relative Permeability Model	*W*	L_1	*G*	L_2*
Number of Grid Cells	500 × 1 × 1					
Porosity	0.20	Residual Saturation	0.4	0.2	0.05	0.05
Permeability	1000 mD	Endpoint Relative Permeability	0.35	0.50	0.65	0.65
		Exponent	3.0	3.0	3.0	3.0
		Initial Saturation	0.4	0.6	0.0	0.0

**W:* Aqueous phase, L_1: Oleic phase, *G:* Gaseous phase, L_2: CO_2-rich liquid phase.

studied so that the phase behavior is accurately represented by one quaternary diagram. For example, in a simulation at the displacement pressure of 1,200 psia, we set the injection well bottomhole pressure to be 1,200 psia and the production-well bottomhole pressure to be 1,190 psia. The injection rate varies with time.

Effect of Pressure on Three-Phase Behavior. We perform a series of simulations of 1D displacements for the BSB-Q oil and injection gas given in Table 2. The displacement pressures are 1,150, 1,200, 1,250, 1,300, and 1,350 psia, and the reservoir temperature is fixed to be 105°F. All the displacements exhibit three-hydrocarbon-phase flow.

Fig. 3 shows the oil recoveries for the five displacements. At displacement pressures of 1,300 and 1,350 psia, the floods are almost piston-like, resulting in a recovery factor of 98%. At 1,200 psia, the displacement is not as efficient, with a recover factor of 80%. The relatively low displacement efficiency is in contrast to Orr and Jensen (1984) and Creek and Sheffield (1993), who related the occurrence of high displacement efficiency to the appearance of the L_2 phase on the *P-x* diagram as part of L_1-L_2-V equilibrium phases. At 1,200 psia, the three-phase region appears on the mixing line between the oil and gas as shown in Fig. 2, but high displacement efficiency is not achieved. This is because a *P-x* diagram does not represent the phase behavior on the composition path actually observed during the displacement.

Fig. 3 also shows L_2 phase mole fractions averaged over the 500 grid cells for the five displacements. The average L_2 phase mole fraction is defined as $\Sigma_k \beta_{L2}/500$, where β_{L2} is the L_2 phase mole fraction in a grid cell and k = 1,…,500. The displacement at 1,200 psia has a larger amount of the L_2 phase than the other displacements, but the recovery factor of 80% is not the highest. That is, the amount of the L_2 phase during a displacement is not a good indicator for high displacement efficiency of low-temperature CO_2 floods.

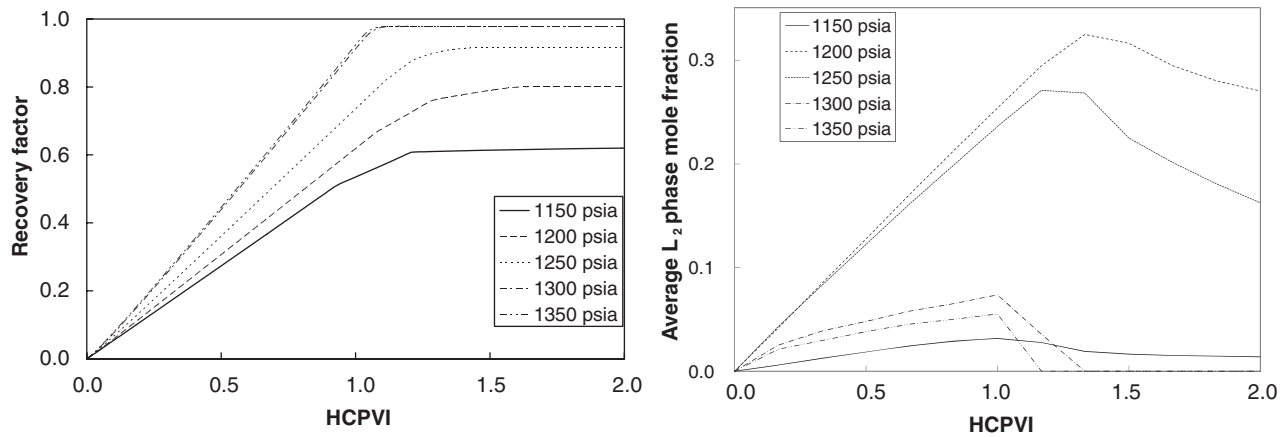

Fig. 3—BSB-Q oil displacements at 105°F for different pressures by the injection gas shown in Table 2. Left: Oil recoveries. Right: L_2 phase mole fractions averaged over the 500 grid cells.

Downloaded from http://onepetro.org/SJ/article-pdf/16/04/751/2106980/spe-129846-pa.pdf/1 by The University of Texas At Austin user on 18 September 2022

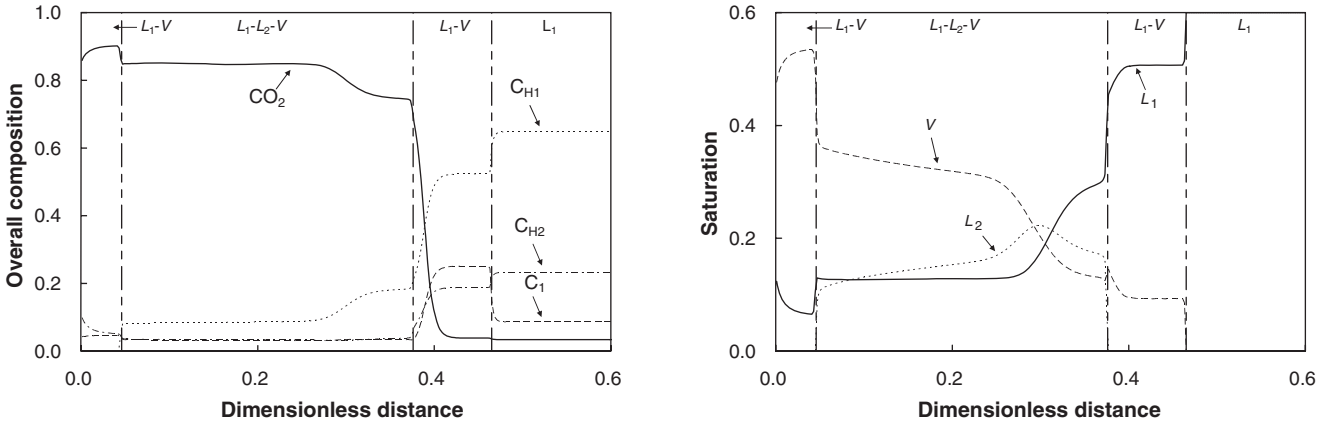

Fig. 4—Physical-property profiles at 0.5 HCPVI for the BSB-Q oil displacement at 105°F and 1,200 psia by the injection gas shown in Table 2. Left: Component concentrations. Right: Phase saturations.

For 1,200 psia, **Fig. 4** gives the profiles of the component concentrations and the phase saturations, respectively, at 0.5 hydrocarbon pore volumes injected (HCPVI). **Fig. 5** shows the entire three-phase region at 105°F and 1,200 psia in BSB-Q composition space. Fig. 5 also shows the composition path, tie lines, and tie triangles along the composition path. The composition path shown in Fig. 5 connects the discrete points of overall compositions simulated at all 500 grid cells. That is, it is an approximate composition path. At the displacement front, the methane bank is generated in the leading L_1-V two-phase region. The front of the three-phase region is where the CO_2 concentration becomes large enough to exhibit the three-hydrocarbon-phase equilibrium at 105°F. The three-phase region along the composition path is shown between the shaded tie triangles in the right portion of Fig. 5. The C_{H1} concentration becomes zero after the three-phase region disappears along the composition path. The L_1-V two-phase region exists over the portion behind the three-phase region. The oscillation near the injection well along the gas tie line is the commonly observed artifact caused by numerical simulation.

For 1,300 psia, **Fig. 6** shows the profiles of the component concentrations and the phase saturations, respectively, at 0.5 HCPVI. The saturation profiles show a sharp reduction in the L_1 phase saturation and a sharp increase in the L_2 phase saturation at the front of the three-phase region. At the tail of the three-phase region, the L_2 phase saturation sharply decreases to zero and the V phase saturation increases by a similar amount. That is, the L_2 phase merges into the V phase and disappears at the tail of the three-phase region.

Fig. 7 shows the three-phase region in composition space at 105°F and 1,300 psia. It also shows the composition path and two- and three-phase regions encountered along the composition path. The significantly elongated tie triangle at the tail of the three-phase region indicates that the composition path goes very near the UCEP tie line. The tie triangle at the front of the three-phase region has a relatively large area, indicating that the composition is not as close to the LCEP tie line as it is to the UCEP tie line.

In Fig. 7, the composition path is affected by dispersion and connects discrete points of overall compositions at the grid cells. This is why the shock from the single-phase region to the two-phase region apparently does not occur along a tie-line extension. In the absence of numerical dispersion, the shock from a single-phase region to a two-phase region must occur along a tie-line extension as proven by Larson (1979).

Fig. 8 compares profiles of phase-composition distances at 0.5 HCPVI at the two different pressures, 1,200 and 1,300 psia. A composition distance between two phases j and k is defined as

$$d_{j-k} = \sqrt{\sum_{i=1}^{N_C} \left(x_{ij} - x_{ik}\right)^2}. \quad \ldots\ldots\ldots\ldots\ldots\ldots\ldots\ldots\ldots\ldots (1)$$

In the figures, $d_{L1\text{-}V}$ represents the distance between the L_1 phase composition and the V phase composition. Similarly, $d_{L1\text{-}L2}$ and $d_{L2\text{-}V}$ represent the distances between the L_1 and L_2 phase compositions and between the L_2 and V phase compositions, respectively. The L_1 phase is immiscible with the V phase over the entire displaced

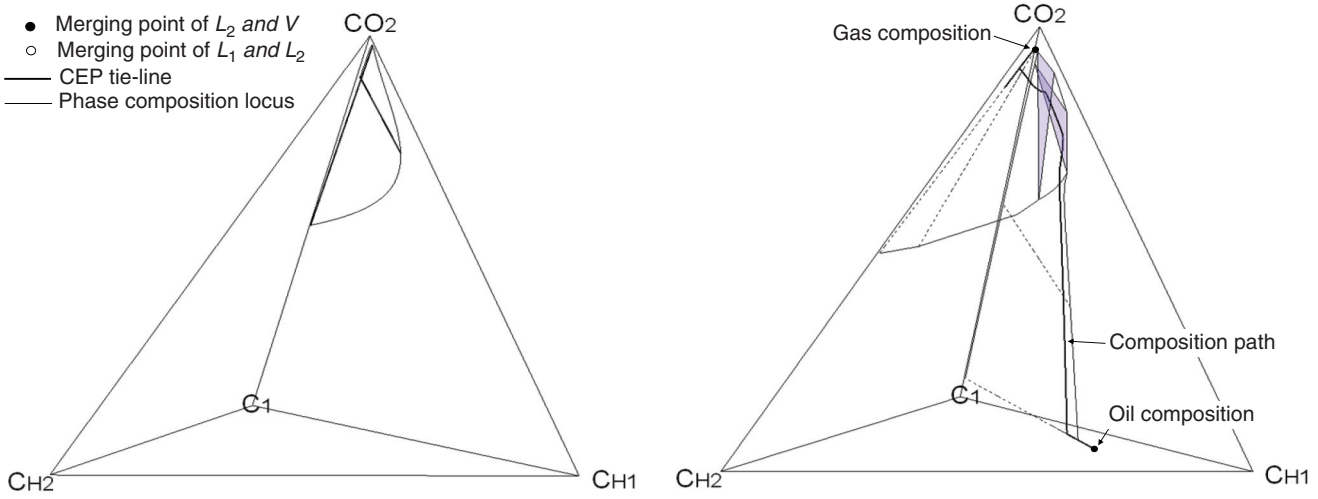

Fig. 5—Left: Three-phase region in BSB-Q composition space at 105°F and 1,200 psia. Right: Simulated composition path and two- and three-phase regions along the composition path for the BSB-Q oil displacement at 105°F and 1,200 psia by the injection gas given in Table 2. 500 grid cells are used for the simulation.

Downloaded from http://onepetro.org/SJ/article-pdf/16/04/751/2106980/spe-129846-pa.pdf/1 by The University of Texas At Austin user on 18 September 2022

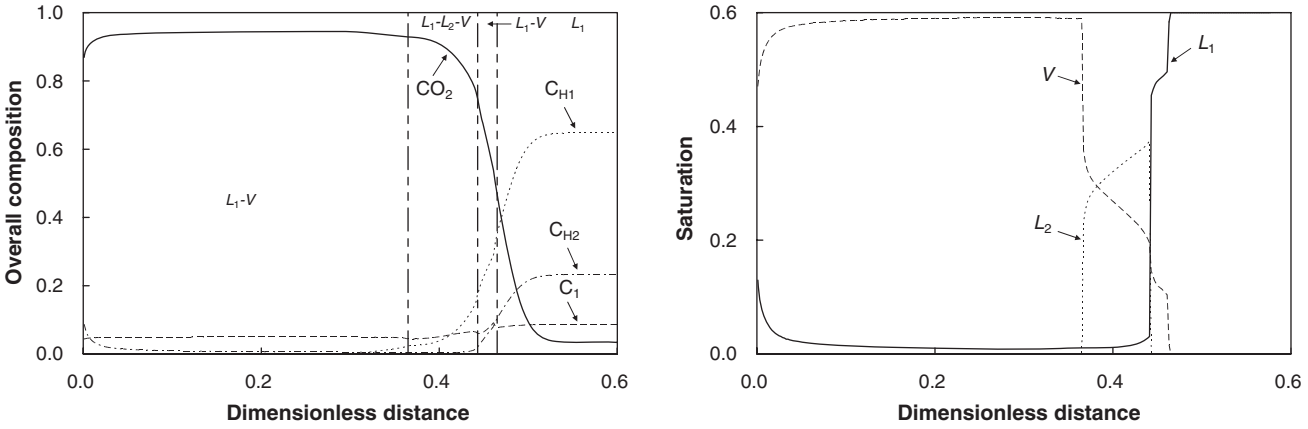

Fig. 6—Physical-property profiles at 0.5 HCPVI for the BSB-Q oil displacement at 105°F and 1,300 psia by the injection gas shown in Table 2. Left: Component concentrations. Right: Phase saturations.

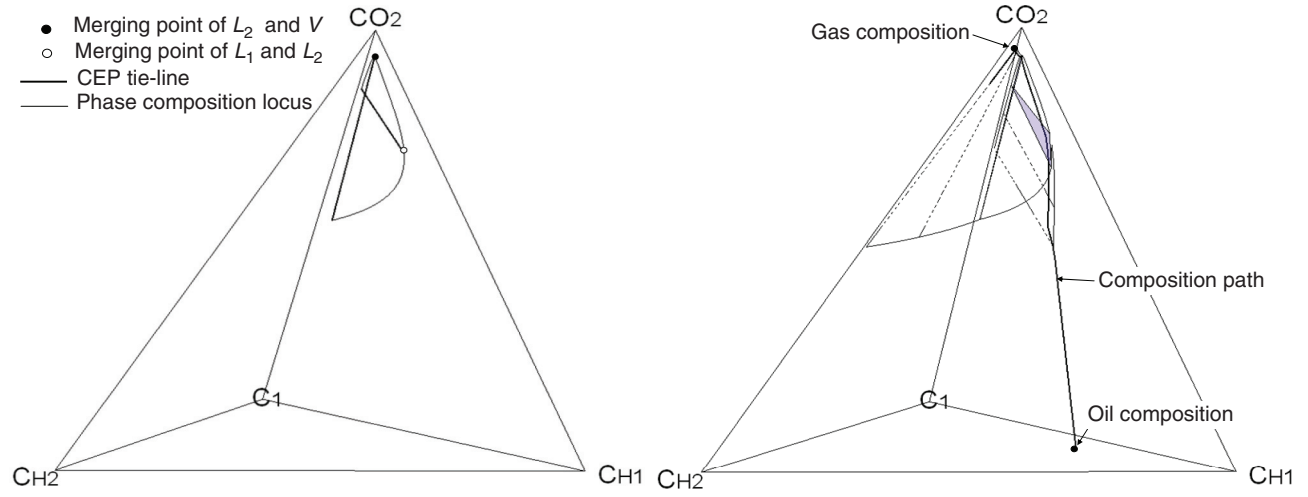

Fig. 7—Left: Three-phase region in BSB-Q composition space at 105°F and 1,300 psia. Right: Simulated composition path and two- and three-phase regions along the composition path for the BSB-Q oil displacement at 105°F and 1,300 psia by the injection gas given in Table 2. 500 grid cells are used for the simulation.

region for all displacements, as indicated by the large $d_{L1\text{-}V}$. At the front of the three-phase region, the degree of criticality between the L_1 and L_2 phases increases as mass transfer between the phases becomes significant. The behavior of $d_{L2\text{-}V}$ significantly changes with pressure. As pressure increases, the composition path goes closer to the UCEP tie line. The value of $d_{L2\text{-}V}$ asymptotically decreases at the tail of the three-phase region for 1,300 psia, resulting in 98% oil recovery.

Fig. 9 shows the oil recoveries, and minimum values of $d_{L1\text{-}L2}$, $d_{L2\text{-}V}$, and $d_{L1\text{-}V}$ along the composition paths for five different pressures. An increase in pressure from 1,300 to 1,350 psia only slightly changes the displacement efficiency. The minimum values

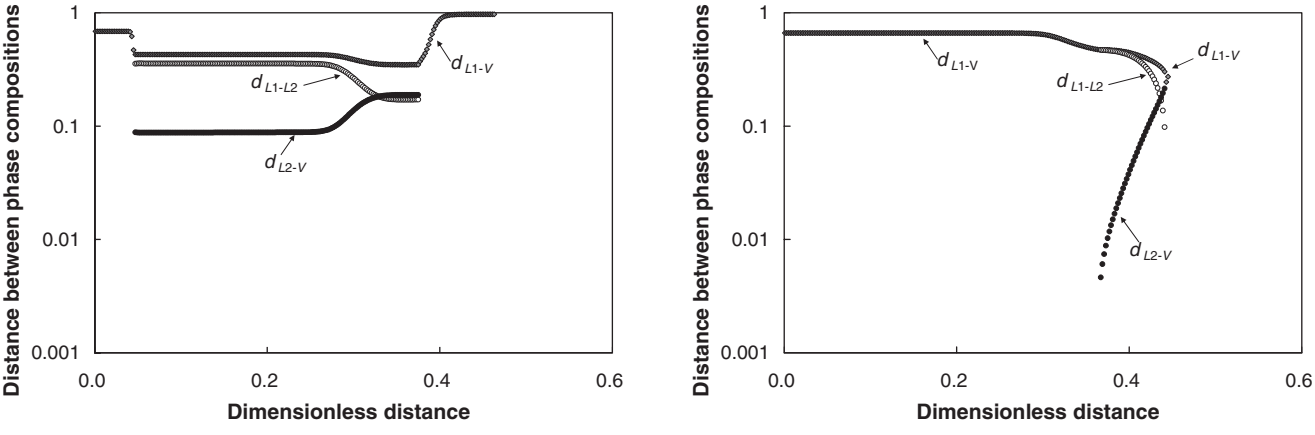

Fig. 8—Distances between phase compositions in composition space at 0.5 HCPVI for the BSB-Q oil displacement at 105°F by the injection gas shown in Table 2. Distance between phase compositions is defined in Eq. 1. Left: 1,200 psia. Right: 1,300 psia.

Downloaded from http://onepetro.org/SJ/article-pdf/16/04/751/2106980/spe-129846-pa.pdf/1 by The University of Texas At Austin user on 18 September 2022

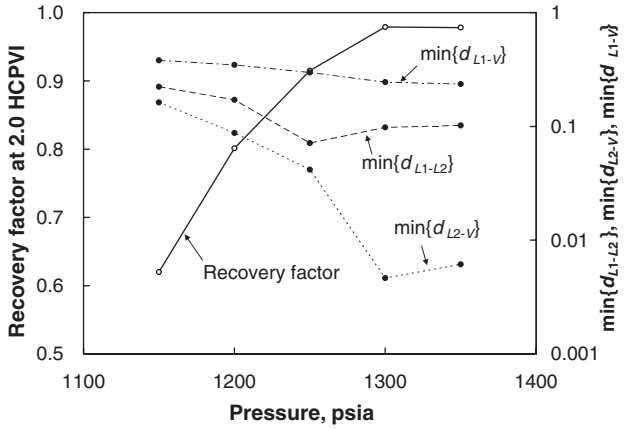

Fig. 9—Oil recoveries at 2.0 HCPVI and minimum values of $d_{L1\text{-}L2}$, $d_{L2\text{-}V}$, and $d_{L1\text{-}V}$ along the composition path for the BSB-Q oil displacements at 105°F by the injection gas shown in Table 2.

of $d_{L1\text{-}L2}$ and $d_{L2\text{-}V}$ do not have a monotonic trend with respect to the displacement pressure. The minimum value of $d_{L2\text{-}V}$, however, monotonically decreases with the increasing recovery factor. That is, oil recovery is increased as the composition path traverses closer to the UCEP tie line. Those results show that the proximity of the composition path to the UCEP tie line controls the displacement efficiency, although the proximity to the LCEP tie line is also important for efficient extraction of oil components by the L_2 phase. The minimum values of $d_{L1\text{-}V}$ are greater than those of $d_{L1\text{-}L2}$ and $d_{L2\text{-}V}$ for all the pressures, indicating that low-temperature CO_2 floods do not require L_1-V miscibility for high displacement efficiency.

Fig. 10 gives a schematic of the role of the CEP behavior in the BSB-Q oil displacement at 1,300 psia. This displacement results in a recovery factor of 98% at 2.0 HCPVI. At the front of the three-phase region, oil components are efficiently extracted by the L_2 phase because of near-miscibility between the L_1 and L_2 phases (i.e., near-LCEP behavior). At the tail of the three-phase region, the L_2 phase disappears, leaving the L_1-V two-phase region behind the three-phase region. When it disappears, the L_2 phase merges into the V phase, instead of into the L_1 phase, for high displacement efficiency. The saturation profiles given in the right portion of Fig. 6 indicate that the L_2 phase merges into the V phase at the trailing edge of the three-phase region. The L_1 phase saturation in the L_1-V two-phase region must be minimized for high displacement efficiency. As the composition path goes closer to the UCEP tie line, the L_1 phase saturation in the L_1-V two-phase region becomes smaller, resulting in higher displacement efficiency. That is, oil components are efficiently extracted from the L_1 into the L_2 phase at the leading edge, and are transferred from the L_2 to the V phase at the trailing edge of the three-phase region. The L_2 phase serves as a buffer between the V and L_1 phases.

Figs. 11a and 11b show component mole fractions in all three phases for the BSB-Q oil displacement at 1,300 psia. We calculate K-values using the component mole fractions shown in Fig. 11 to illustrate further the displacement mechanisms. There are three kinds of K-values; $K_{iV/L1} = x_{iV}/x_{iL1}$, $K_{iV/L2} = x_{iV}/x_{iL2}$, and $K_{iL2/L1} = x_{iL2}/x_{iL1}$, where x_{ij} is the mole fraction of component i in phase j, $i = 1,\ldots,N_C$, and $j = \{V, L_1, L_2\}$. For vaporizing behavior, K-values diverge away from each other from the downstream to the upstream. Condensing behavior exhibits converging K-values in the same direction.

Fig. 12 gives the K-value profiles for the BSB-Q oil displacement at 1,300 psia. As $K_{V/L1}$ indicates, CO_2 is condensed from the V into the L_1 phase in the two-phase region ahead of the three-phase region, while CO_2 is vaporized from the L_1 phase into the V phase in the two-phase region behind the three-phase region. $K_{V/L2}$ and $K_{L2/L1}$ indicate that condensing and vaporizing behavior of intermediate components occur simultaneously within the three-phase region.

Vaporizing behavior occurs when the distance between equilibrium-phase compositions increases from the downstream to the upstream, while condensing behavior occurs when the distance decreases in the same direction. The simultaneous condensing/vaporizing behavior within the three-phase region is also shown in Fig. 8, where $d_{L1\text{-}L2}$ increases and $d_{L2\text{-}V}$ decreases from the downstream to the upstream. The $d_{L1\text{-}V}$ profile also indicates condensation in the leading two-phase region and vaporization in the trailing two-phase region.

Gardner et al. (1981) concluded that their low-temperature oil displacement by CO_2 is a vaporizing gas drive, in which oil components are extracted (or "vaporized") into the L_2 phase. This is in contrast to Metcalfe and Yarborough (1979), who stated that low-temperature oil displacement by CO_2 is a condensing gas drive, where CO_2 is condensed into the L_1 phase. The complex mass-transfer mechanisms among the three phases shown in Figs. 8 and 12 were not identified by these authors.

Fig. 12 also demonstrates that use of K-values can be misleading to identify the degree of miscibility between phases. For example, based on the $K_{V/L1}$ profiles, the shortest tie line occurs at a dimensionless distance of 0.365, where L_1-V two phases are present immediately behind the three-phase region. However, the shortest tie line actually occurs at a dimensionless distance of 0.443, which is just ahead of the three-phase region. The $K_{V/L1}$-values are (1.66, 2.66, 1.22×10^{-1}, 1.77×10^{-4}) at 0.365 and (1.18, 2.66, 5.77×10^{-2}, 3.58×10^{-5}) at 0.443. $d_{L1\text{-}V}$ is 0.472 at a dimensionless distance of

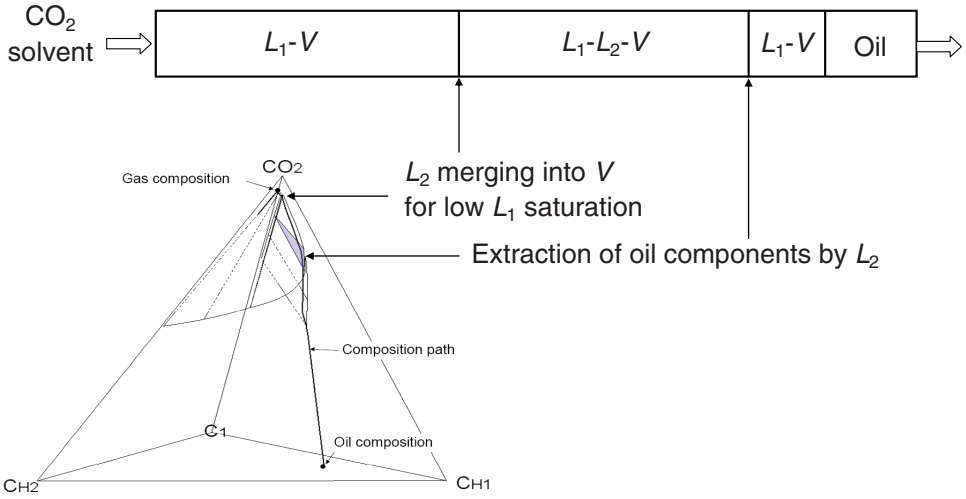

Fig. 10—Illustration of CEP behavior for the BSB-Q oil displacement at 105°F and 1,300 psia by the injection gas of Table 2.

Downloaded from http://onepetro.org/SJ/article-pdf/16/04/751/2106980/spe-129846-pa.pdf/1 by The University of Texas At Austin user on 18 September 2022

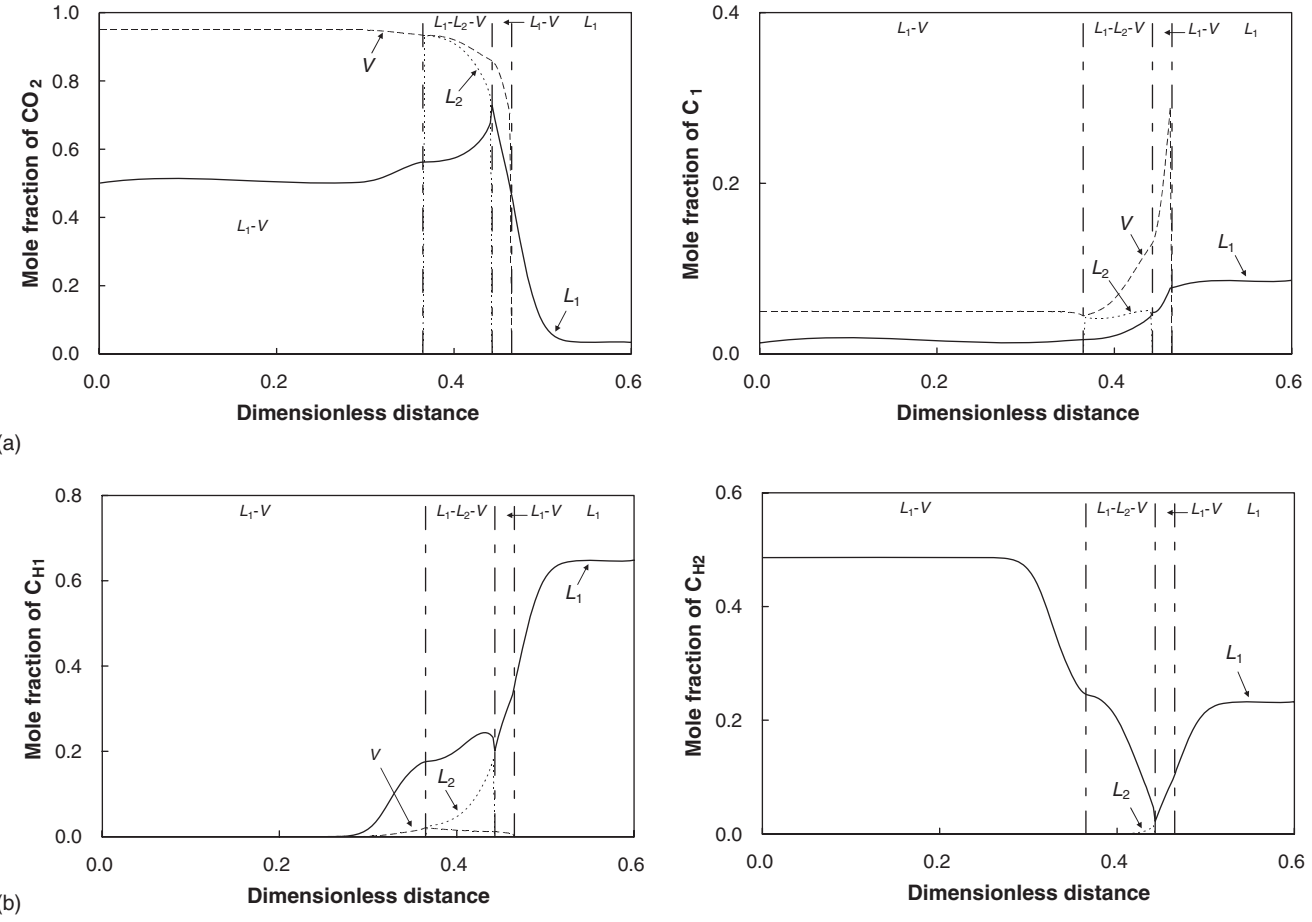

Fig. 11—(a) Component mole fractions in all phases at 0.5 HCPVI for the BSB-Q oil displacement at 105°F and 1,300 psia by the injection gas shown in Table 2. Left: CO_2 mole fractions. Right: C_1 mole fractions. (b) Component mole fractions in all phases at 0.5 HCPVI for the BSB-Q oil displacement at 105°F and 1,300 psia by the injection gas shown in Table 2. Left: C_{H1} mole fractions. Right: C_{H2} mole fractions.

0.365 and is 0.245 at a distance of 0.443. $d_{L1\text{-}V}$ in Fig. 8 correctly shows that the shortest tie line is at a dimensionless distance of 0.443, not at 0.365. Therefore, we use distances between equilibrium-phase compositions, instead of *K*-values, to identify the degree of miscibility between the phases at a fixed temperature and pressure.

Effect of Oil Characterization on Three-Phase Behavior. This section examines how the three-phase region changes as the properties of the heavy components (C_{H1} and C_{H2}) of the BSB-Q oil are adjusted. The fluid-characterization procedure of Pedersen et al. (1984a, b; 1985; 1992; 2004) and Pedersen and Christensen (2007) is used to change the oil properties in a systematic way.

Oil Characterizations. The carbon numbers for C_{H1} and C_{H2} for the BSB-Q oil are calculated from the molecular weights using the equation of Pedersen et al.: $MW_i = 14C_i - 4$. MW_i and C_i are the molecular weight and carbon number of component *i*, respectively. The carbon numbers calculated for C_{H1} and C_{H2} are 7.32 and 25.59, respectively. The temperature is fixed at 105°F for the various oils.

We generate three different oils: one lighter oil (BSB-QL) and two heavier oils (BSB-QH1 and BSB-QH2), compared with the BSB-Q oil. For the BSB-QL oil, the carbon numbers for C_{H1} and C_{H2} in the BSB-Q oil are multiplied by 0.75, resulting in the carbon numbers 5.49 and 19.20. For the BSB-QH1 oil, the multiplication factor is 1.25 to obtain the carbon numbers 9.15 and 31.98 for C_{H1} and C_{H2}, respectively. For the BSB-QH2 oil, a multiplication factor of 1.5 is used, which results in the carbon numbers 10.98 for C_{H1} and 38.38 for C_{H2}. Those carbon numbers are then used to calculate EOS parameters, such as critical temperature (T_C), critical pressure (P_C), and acentric factors, based on the procedure given in Pedersen et al. The BICs are the same as those for the BSB-Q oil because there are no widely accepted correlations for BICs for mixtures consisting of more than two components. Viscosity calculations in UTCOMP also require the critical volumes for the components. The critical volumes for C_{H1} and C_{H2} are calculated using the correlation of Riazi and Daubert (1980) together with the correlation of Katz and Firoozabadi (1978) for boiling points. The resulting properties for the BSB-QL, BSB-QH1, and BSB-QH2 oils are summarized in **Tables 4 through 6,** respectively.

The procedure described previously generates different oils for fixed oil and injection-gas compositions. Another way to generate different oils is to change the composition of the BSB-Q oil. We use the former approach because it shows more clearly the composition effects on the phase behavior and displacement path taken in composition space.

The behavior of a fluid for a two-parameter cubic EOS is determined by the attraction parameter ("*a* parameter") and the covolume parameter ("*b* parameter"), which are calculated using T_C, P_C, and the acentric factor assigned to each component. For a mixture, the *a* and *b* parameters for the components are used to calculate the parameters for the mixture, a_m and b_m, based on mixing rules with BICs. Dissimilarity between the oil and injection gas can be measured by comparing the parameters a_m and b_m for the oil and those for the injection gas. We define a dimensionless dissimilarity parameter ξ as

$$\xi = \left[\left(\frac{a_m}{b_m}\right)_{\text{Oil}} - \left(\frac{a_m}{b_m}\right)_{\text{Gas}}\right] \Big/ \left[\left(\frac{a_m}{b_m}\right)_{\text{Oil}} + \left(\frac{a_m}{b_m}\right)_{\text{Gas}}\right]. \quad \ldots\ldots\ldots (2)$$

Downloaded from http://onepetro.org/SJ/article-pdf/16/04/751/2106980/spe-129846-pa.pdf/1 by The University of Texas At Austin user on 18 September 2022

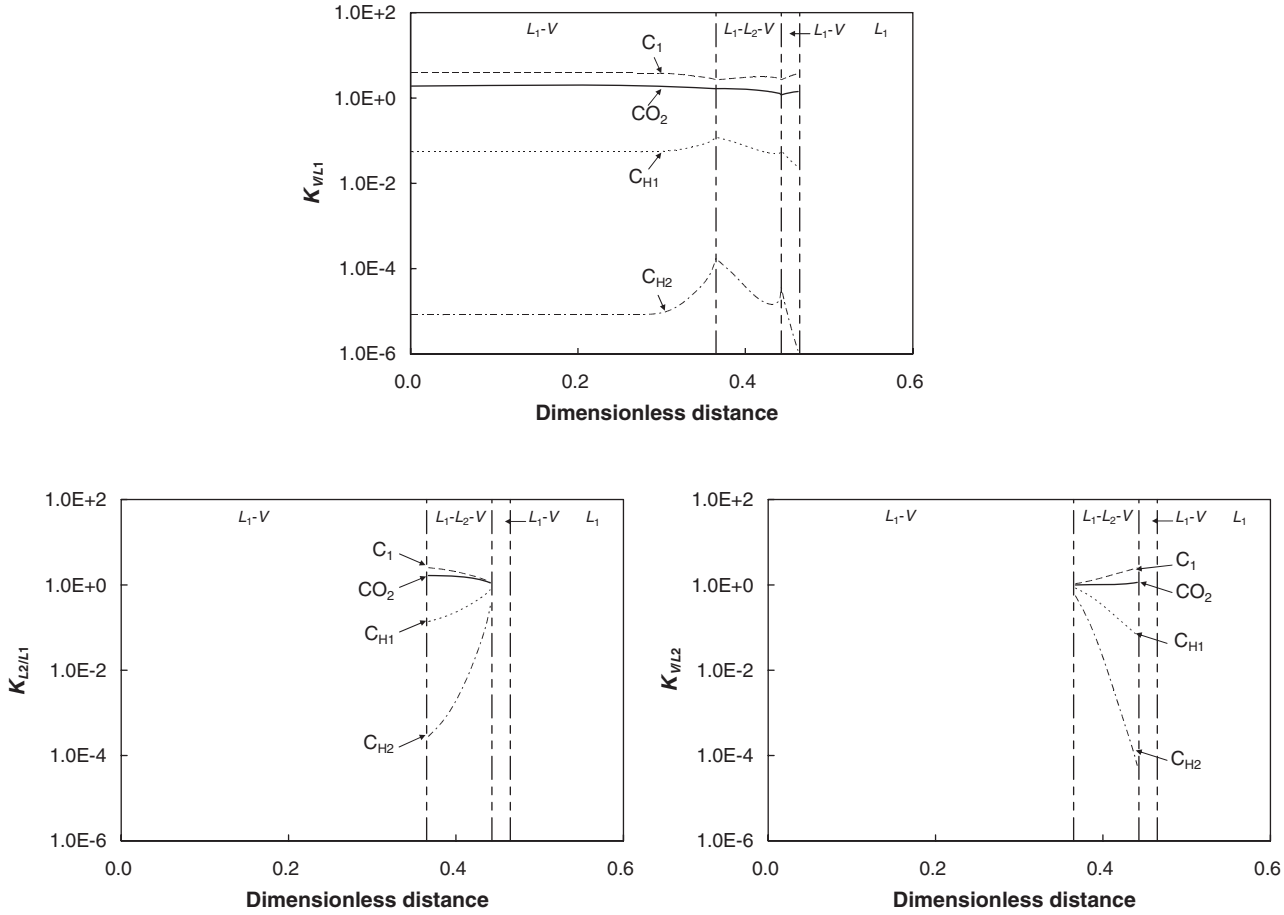

Fig. 12—*K*-value profiles at 0.5 HCPVI for the BSB-Q oil displacement at 105°F and 1,300 psia by the injection gas shown in Table 2. Top: $K_{iV/L1}$ defined as x_{iV}/x_{iL1}. Bottom left: $K_{iL2/L1}$ defined as x_{iL2}/x_{iL1}. Bottom right: $K_{iV/L2}$ defined as x_{iV}/x_{iL2}.

Eq. 2 is similar to one of the dimensionless parameters introduced by van Konynenburg and Scott (1980) to characterize binary mixtures. The main difference here is that we use mixing rules to characterize the fluid, and we consider the oil and gas as pseudocomponents. The parameter ξ is zero when the oil has the same properties as the injection gas, and it approaches 1.0 as the oil becomes heavier. The advantage of using the dissimilarity parameter over using a carbon number is that the former accounts

TABLE 4—FLUID PROPERTIES FOR THE BSB-QL OIL

	Molecular Weight	T_C (°F)	P_C (psia)	Acentric Factor	V_C (ft^3/lb-mol)
C_{H1}	72.84	415.57	520.95	0.259	4.36
C_{H2}	264.65	909.90	225.44	0.851	17.21

*Oil/gas compositions, *h*, *g*, and BICs are the same as the BSB-Q oil in Table 2.

TABLE 5—FLUID PROPERTIES FOR THE BSB-QH1 OIL

	Molecular Weight	T_C (°F)	P_C (psia)	Acentric Factor	V_C (ft^3/lb-mol)
C_{H1}	124.07	594.19	352.01	0.430	7.81
C_{H2}	443.75	1212.83	188.40	1.216	29.09

*Oil/gas compositions, *h*, *g*, and BICs are the same as the BSB-Q oil in Table 2.

TABLE 6—FLUID PROPERTIES FOR THE BSB-QH2 OIL

	Molecular Weight	T_C (°F)	P_C (psia)	Acentric Factor	V_C (ft^3/lb-mol)
C_{H1}	149.68	663.31	308.82	0.513	9.53
C_{H2}	533.30	1348.76	180.25	1.286	35.01

*Oil/gas compositions, *h*, *g*, and BICs are the same as the BSB-Q oil in Table 2.

Downloaded from http://onepetro.org/SJ/article-pdf/16/04/751/2106980/spe-129846-pa.pdf/1 by The University of Texas At Austin user on 18 September 2022

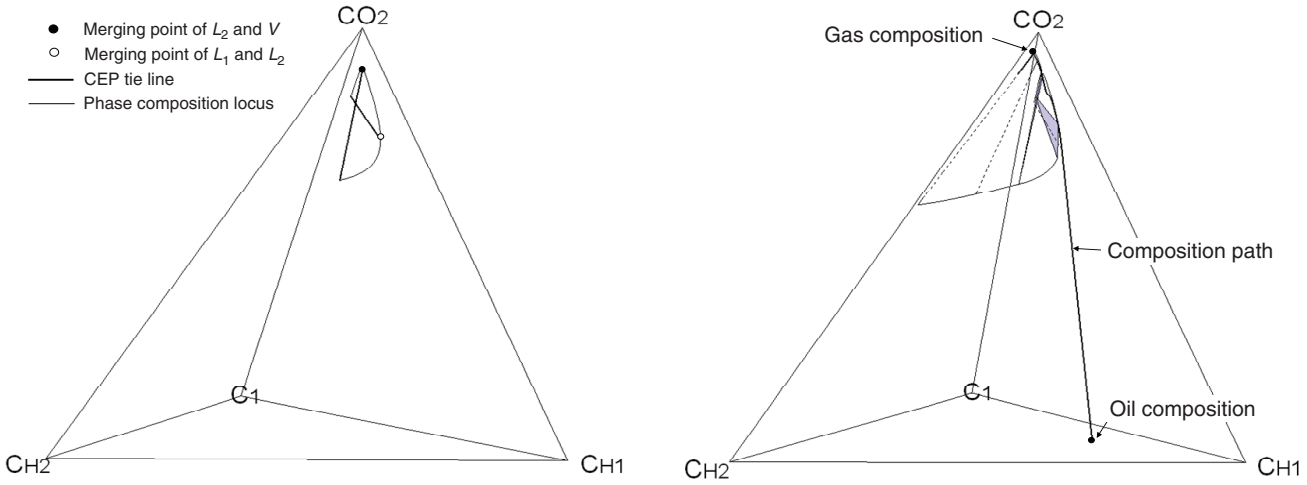

Fig. 13—Left: Three-phase region in BSB-QL composition space at 105°F and 1,300 psia. The component properties are given in Table 4. Right: Simulated composition path and two- and three-phase regions along the composition path for the BSB-QL oil displacement at 105°F and 1,300 psia.

for the dependence of the EOS results on the correlations used for T_C, P_C and acentric factors.

The oils BSB-QL, BSB-QH1, and BSB-QH2 have different dissimilarity values ξ. The parameters a_m and b_m for the injection gas are fixed because the injection-gas components are held constant (i.e., the gas consists of only CO_2 and C_1). The parameter ξ depends on temperature through the attraction parameter; but at first, temperature is constant.

The parameter ξ using the Peng-Robinson EOS at 105°F is calculated to be 0.498 for the BSB-QL/solvent system given in Table 4, 0.649 for the BSB-QH1/solvent system given in Table 5, and 0.691 for the BSB-QH2/solvent system given in Table 6. For the BSB-Q oil/solvent system in Table 2, ξ is 0.573.

Three-Phase Region and Displacement Efficiency. Figs. 13 and 14 show the three-phase regions at 105°F and 1,300 psia for the two different quaternary oil displacements: BSB-QL (ξ = 0.498) and BSB-QH2 (ξ = 0.691), respectively. Fig. 7 shows the three-phase region at the same *P–T* conditions for the oil BSB-Q (ξ = 0.573). Immiscibility between the three phases increases with increasing ξ. That is, the length of the CEP tie lines increases with ξ.

Fig. 15 shows the *P–x* diagram at 105°F and *P–T* projection for the pseudobinary mixture of the BSB-QL oil and injection gas (Table 4). Similarly, **Figs. 16 and 17** give these same properties for the BSB-QH1 oil (Table 5) and BSB-QH2 oil (Table 6), respectively. The *P–x* diagram and *P-T* projection for the BSB-Q oil were previously presented in Fig. 2. On the *P-x* diagrams, the two- and three-phase immiscibility increases as ξ increases. For example, the three-phase region exists at solvent mole fractions between 0.71 and 0.93 for the BSB-QL system, while it exists at solvent mole fractions between 0.57 and 0.98 for the BSB-QH2 system. The increasing immiscibility with ξ is more obvious in the *P–T* projections. For the BSB-QL system, the critical locus goes near the critical point of the solvent to exhibit a minimum in pressure. However, as ξ increases, the critical locus systematically shifts to higher temperature, and there is no minimum pressure observed on the critical locus for the BSB-QH2 system. Also, the three-phase region becomes larger as ξ increases.

We simulated 1D displacements of the BSB-QL and BSB-QH2 oils at different pressures at 105°F. All displacements studied exhibit three-hydrocarbon-phase flow similar to the BSB-Q oil cases presented before. Displacements of the BSB-QL and BSB-QH2 oils achieve a high displacement efficiency by the same mechanism described for the BSB-Q oil. **Fig. 18** summarizes the relationship between the oil recoveries at 2.0 HCPVI and proximity of the composition path to the UCEP tie line (as measured by $\min\{d_{L2\text{-}V}\}$) for the displacements of BSB-QL, BSB-Q, and BSB-QH2 at 105°F. The plots confirm that those displacements become

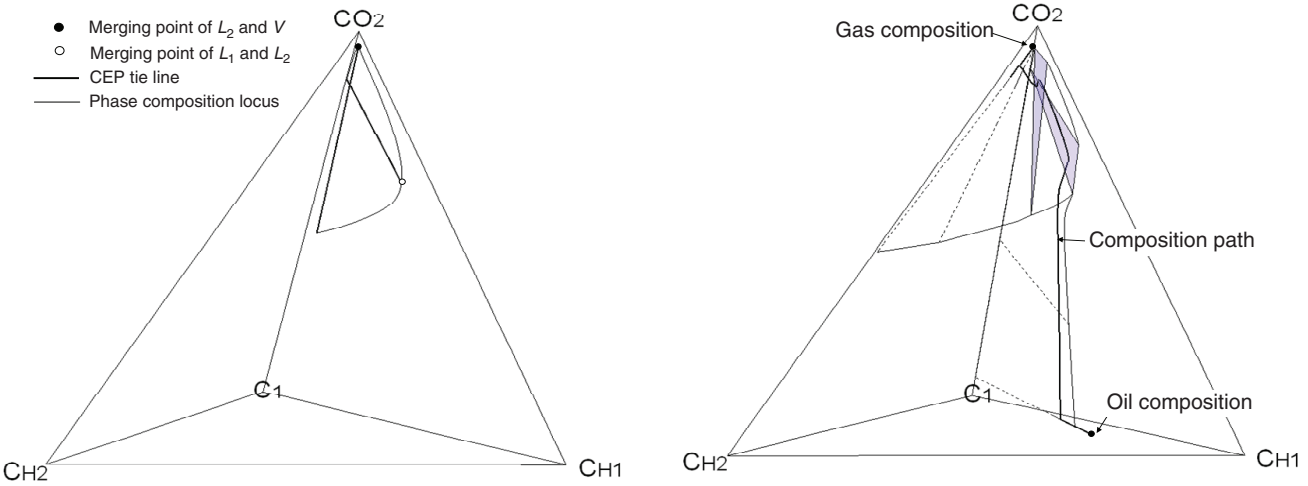

Fig. 14—Left: Three-phase region in BSB-QH2 composition space at 105°F and 1,300 psia. The component properties are given in Table 6. Right: Simulated composition path and two- and three-phase regions along the composition path for the BSB-QH2 oil displacement at 105°F and 1,300 psia.

Downloaded from http://onepetro.org/SJ/article-pdf/16/04/751/2106980/spe-129846-pa.pdf/1 by The University of Texas At Austin user on 18 September 2022

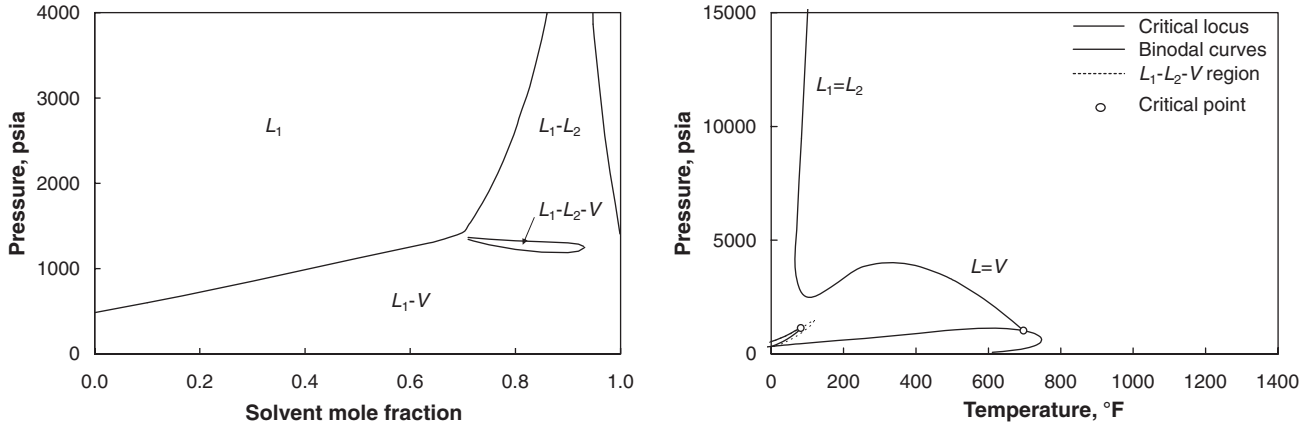

Fig. 15—Phase diagrams for the pseudobinary mixture of the BSB-QL oil and injection gas given in Table 4. Left: *P–x* diagram at 105°F. Right: *P–T* projection of the *P–T–x* diagram.

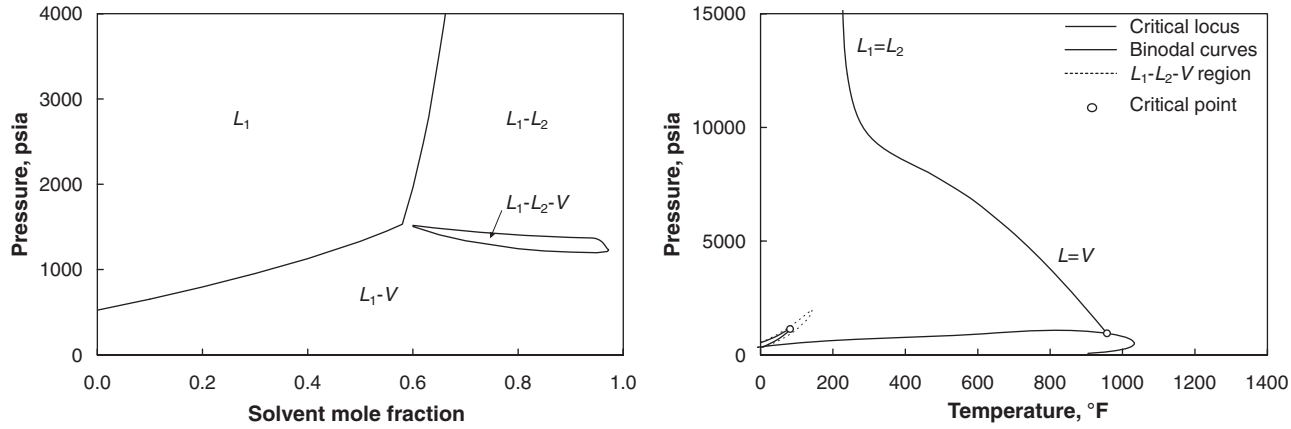

Fig. 16—Phase diagrams for the pseudobinary mixture of the BSB-QH1 oil and injection gas given in Table 5. Left: *P–x* diagram at 105°F. Right: *P–T* projection of the *P–T–x* diagram.

more efficient when the composition path goes closer to the UCEP tie line. Fig. 18 also shows that displacement efficiency is less correlated with the proximity of the composition path to the LCEP tie line than with proximity to the UCEP tie line. Close proximity to the LCEP tie line, however, is also necessary for the efficient extraction of oil components into the L_2 phase at the leading edge of the three-phase region.

The composition paths at 1,300 psia and 105°F for the BSB-QL (Fig. 13), BSB-Q (Fig. 7), and BSB-QH2 oils (Fig. 14) demonstrate that the nature of the oil significantly affects the displacements because of the different three-phase regions encountered. As ξ decreases at a fixed temperature and pressure, the composition path goes closer to the UCEP tie line, resulting in more efficient displacement. This is in contrast to the findings of Yellig and Metcalfe (1980), who concluded that the efficiency of low-temperature oil displacements by CO_2 is little affected by oil properties. **Fig. 19** shows that the displacement pressure that results in a recovery factor of 97% at 2.0 HCPVI (P_1 in Fig. 19) increases with the dissimilarity between the oil and injection gas (i.e., ξ defined in Eq. 2). The oil properties affect the displacement

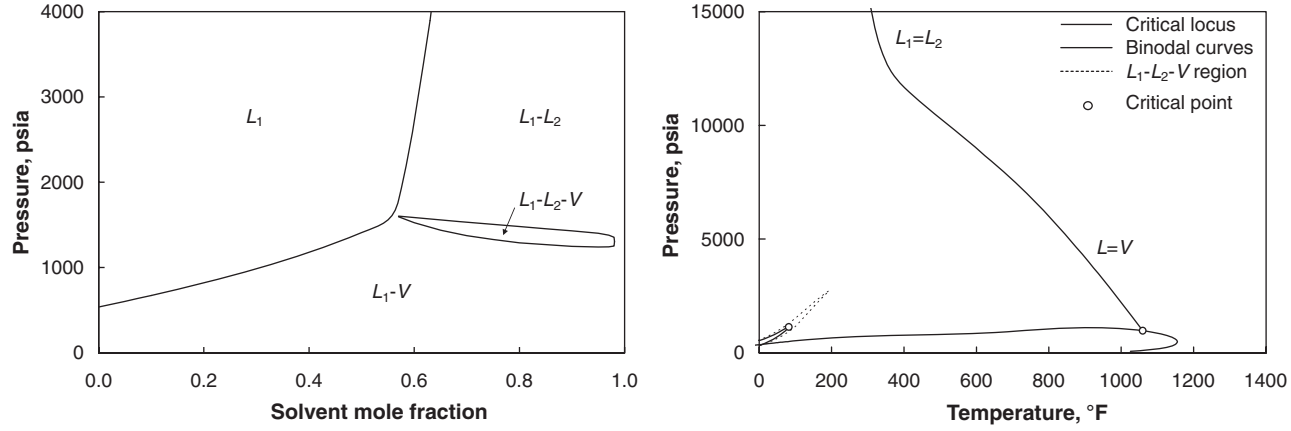

Fig. 17—Phase diagrams for the pseudobinary mixture of the BSB-QH2 oil and injection gas given in Table 6. Left: *P–x* diagram at 105°F. Right: *P–T* projection of the *P–T–x* diagram.

Downloaded from http://onepetro.org/SJ/article-pdf/16/04/751/2106980/spe-129846-pa.pdf/1 by The University of Texas At Austin user on 18 September 2022

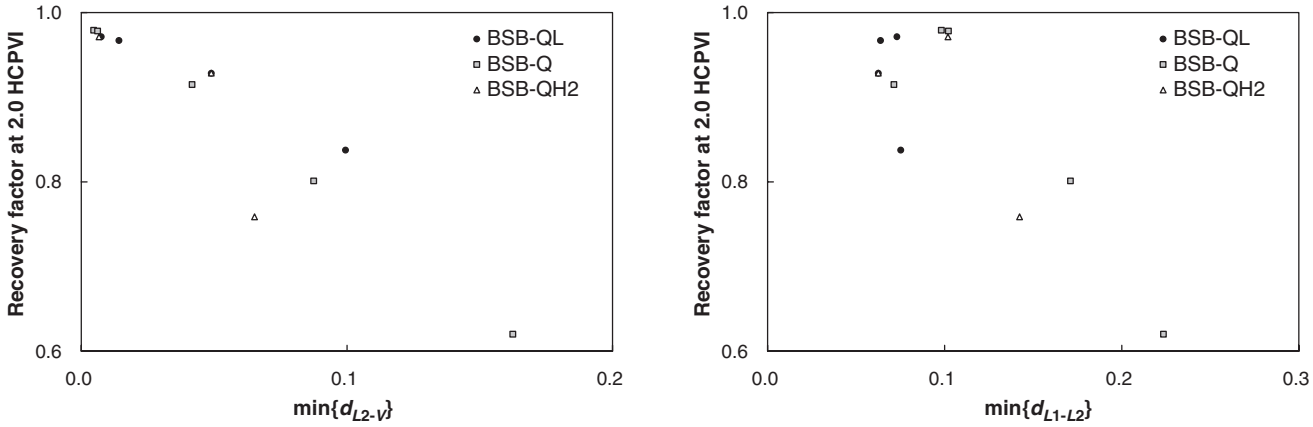

Fig. 18—Oil recoveries at 2.0 HCPVI for the BSB-QL, BSB-Q, and BSB-QH2 displacements at 105°F. Left: With respect to the minimum value of $d_{L2\text{-}V}$ along the composition path. Right: With respect to the minimum value of $d_{L1\text{-}L2}$ along the composition path.

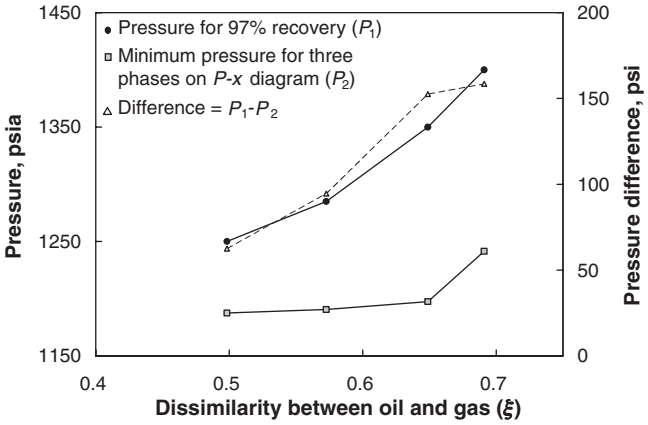

Fig. 19—Displacement pressures required for a recovery factor of 97% at 2.0 HCPVI (P_1) and the minimum pressures that bound the three-phase region on P-x diagrams (P_2) at 105°F for four different oil/injection-gas pairs; BSB-QL (ξ = 0.498), BSB-Q (ξ = 0.573), BSB-QH1 (ξ = 0.649), and BSB-QH2 (ξ = 0.691). Pressure difference on the right y-axis is defined as ($P_1 - P_2$). Parameter ξ is defined in Eq. 2.

efficiency because they can significantly change the three-phase behavior and, therefore, the composition path taken.

Fig. 19 also shows the minimum pressures at which three phases appear on P–x diagrams (P_2 in Fig. 19) for different ξ values. At the minimum pressures, the mixing line between the oil and injection gas is tangent to the three-phase region in composition space. P_2 is lower than P_1 for the four oils studied here. The difference between the two pressures, P_1–P_2, becomes larger as ξ increases. The difference is 63 psi for ξ = 0.498 (BSB-QL) and 159 psi for ξ = 0.691 (BSB-QH2). Orr and Jensen (1984) and Creek and Sheffield (1993) considered that the efficiency of low-temperature oil displacement by CO_2 is related to the appearance of three phases on a P–x diagram. However, displacement efficiency is determined by interaction between flow and phase behavior along its displacement path, instead of by the phase behavior on a P-x diagram. Therefore, the MMP as sometimes defined by the lower bound of the three phase region on a P–x diagram could be in error, and in some cases the three-phase region may be missing on a P–x diagram even though it is present during a displacement. The importance of considering phase behavior along the displacement path and not the P–x diagram should also be taken into account in EOS fluid characterization for gasflooding simulation.

Effect of Temperature on Three-Phase Behavior. In this section, we examine the effect of temperature on displacement efficiency. **Fig. 20** shows the P-x diagrams of the BSB-Q oil and injection gas in Table 2 at 90°F and 120°F. The three-phase region exists in a pressure range from 998 to 1,310 psia at solvent concentrations between 0.64 and 0.99 for 90°F. For 120°F, the three-phase region exists in a pressure range from 1,411 to 1,660 psia at solvent concentrations between 0.63 and 0.91.

We simulated 1D displacements of the BSB-Q oil by the injection gas given in Table 2 at 90°F and 120°F. The reservoir properties are shown in Table 3. The results were compared with those at 105°F presented in a previous section. **Fig. 21** summarizes the oil recoveries at 2.0 HCPVI for a series of displacements at different pressures and temperatures. The results show that oil

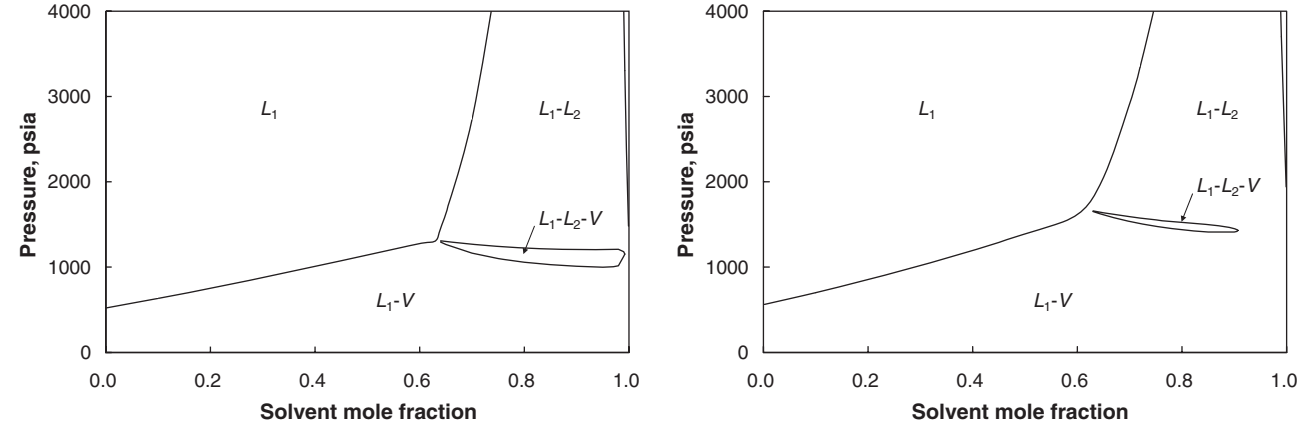

Fig. 20—P–x diagrams for the BSB-Q oil and injection gas given in Table 2. Left: 90°F. Right: 120°F.

Downloaded from http://onepetro.org/SJ/article-pdf/16/04/751/2106980/spe-129846-pa.pdf/1 by The University of Texas At Austin user on 18 September 2022

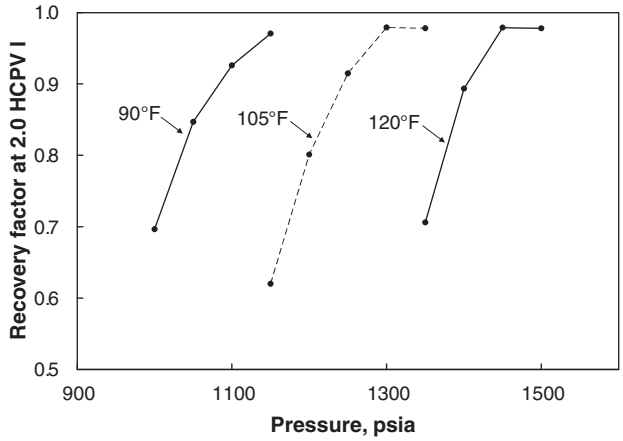

Fig. 21—Oil recoveries at 2.0 HCPVI at different pressures and temperatures for the BSB-Q oil displacement. The fluid properties are given in Table 2.

recovery significantly depends on reservoir temperature. This is consistent with the observations of Holm and Josendal (1974), Yellig and Metcalfe (1980), and Orr and Jensen (1984), who related the CO_2 MMP to reservoir temperature. **Fig. 22** shows the three-phase regions in BSB-Q composition space at 1,300 psia and 90 and 120°F. Comparison of Fig. 22 with the three-phase region at 105°F in Fig. 7 illustrates that three-phase behavior at a fixed pressure can significantly change. More details of the three-phase behavior for these quaternary systems are given in Okuno (2009).

Fig. 23 shows the recovery factors at 2.0 HCPVI with respect to the minimum value of $d_{L2\text{-}V}$ along the composition paths at different displacement pressures and reservoir temperatures for the BSB-Q oil displacements. Similarly, oil recoveries at 2.0 HCPVI with respect to the minimum value of $d_{L1\text{-}L2}$ are given in Fig. 23. For different reservoir temperatures, the BSB-Q oil displacements achieve higher displacement efficiency when the composition path goes closer to the UCEP and LCEP tie lines. However, the value of $\min\{d_{L2\text{-}V}\}$ (i.e., proximity to the UCEP tie line) is more important for high displacement efficiency than the value of $\min\{d_{L1\text{-}L2}\}$ (i.e., proximity to the LCEP tie line) based on the results presented. Figs. 18 and 23 show that the recovery factor at 2.0 HCPVI is more than 96% when $\min\{d_{L2\text{-}V}\}$ is less than 0.02 for the displacements of the BSB-Q oil at 90, 105, and 120°F and the BSB-QL and BSB-QH2 oils at 105°F.

Case Study Using the BSB Oil

In the quaternary models, we showed that three-hydrocarbon-phase flow can achieve high displacement efficiency when oil components transfer efficiently from the L_1 to the V phase with the L_2 phase as a buffer between them. This mass transfer occurs when the composition path traverses near the UCEP and LCEP tie lines.

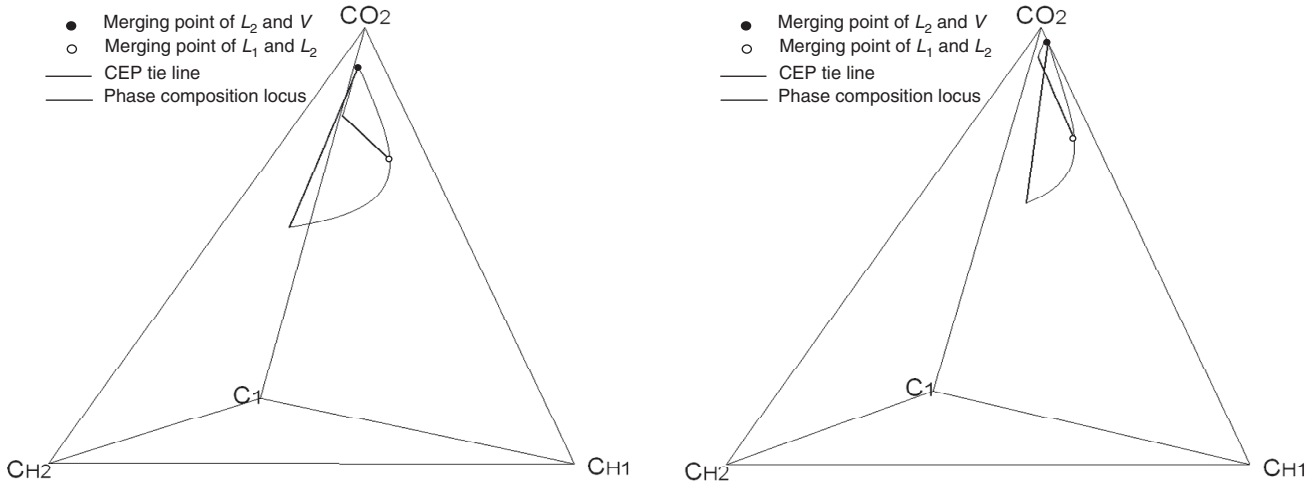

Fig. 22—Three-phase region in BSB-Q composition space at 1,300 psia. The component properties are given in Table 2. Left: 90°F. Right: 120°F.

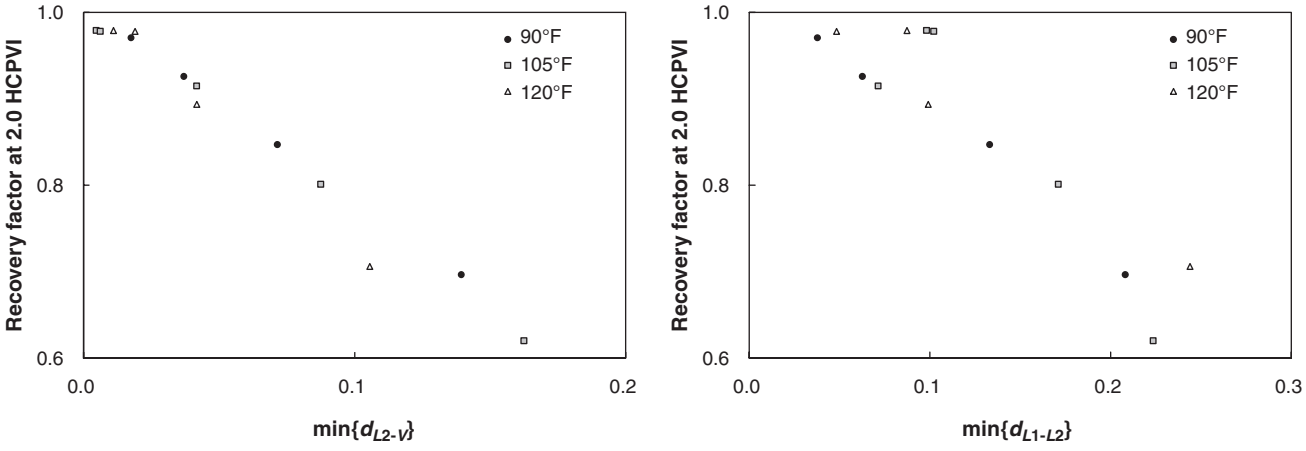

Fig. 23—Left: Oil recoveries at 2.0 HCPVI with respect to the minimum values of $d_{L2\text{-}V}$ along the composition path for the BSB-Q oil displacements at different pressures and temperatures. Right: Oil recoveries at 2.0 HCPVI with respect to the minimum values of $d_{L1\text{-}L2}$ along the composition path for the BSB-Q oil displacements at different pressures and temperatures.

Downloaded from http://onepetro.org/SJ/article-pdf/16/04/751/2106980/spe-129846-pa.pdf/1 by The University of Texas At Austin user on 18 September 2022

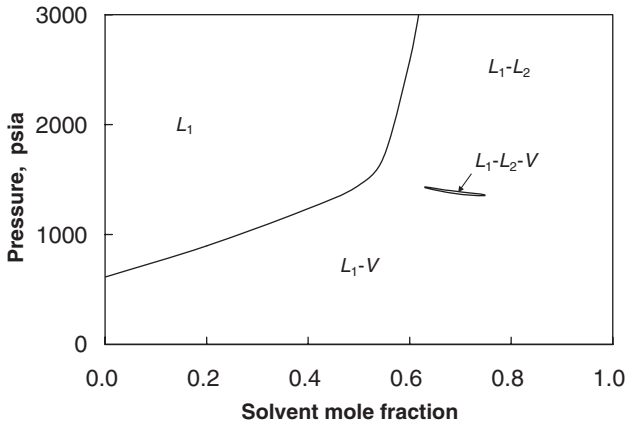

Fig. 24—*P–x* diagram at 105°F for the BSB oil and injection gas given in Table 1.

In this section, we show that displacement using the seven-component BSB oil in west Texas also achieves high displacement efficiency as a result of the same displacement mechanism. Although not shown in this paper, the same displacement mechanism occurs for other oils such as the Monahans Clearfork oil (Lim et al. 1992), the North Ward Este oil, the JEMA oil, and Oil G (Khan et al. 1992). Details of those displacements can be found in Okuno (2009).

The BSB oil is a west Texas oil with a reservoir temperature of 105°F. Khan et al. (1992) characterized the BSB oil using the Peng-Robinson EOS, for which the EOS parameters are given in Table 1. Parameters h and g are also given for use of a rapid and robust reduced method described in Okuno (2009) and Okuno et al. (2010b, c).

We consider BSB oil displacements by the injection gas (95% CO_2 and 5% C_1) given in Table 1. **Fig. 24** shows the P–x diagram at the reservoir temperature of 105°F for pseudobinary mixtures of the BSB oil with solvent. The three-phase region exists in a narrow pressure range from 1,354 to 1,433 psia on the P–x diagram. However, as will be presented next, three-phase equilibrium occurs in a much wider pressure range during the displacements because the P–x diagram represents phase behavior only along the mixing line between the oil and injection gas, instead of along the actual composition path.

Fig. 25 shows oil recoveries for the 1D displacements at five different pressures; 1,150, 1,200, 1,250, 1,300, and 1,350 psia. All the displacements exhibit immiscible three-hydrocarbon-phase flow even though the pressure range for the three phases in Fig. 24 is only from 1,354 to 1,433 psia. The displacement at 1,300 psia results in 93% oil recovery at 2.0 HCPVI. The increment in oil recovery becomes marginal above 1,300 psia, as shown in Fig. 25. The displacement at 1,350 psia recovers 94% of the original oil, only 1% greater recovery compared with 1,300 psia.

Figs. 26 and 27 show phase saturation profiles at 0.5 HCPVI for the displacements at 1,150 and 1,300 psia, respectively. The oscillation near the injection well is an artifact caused by numerical

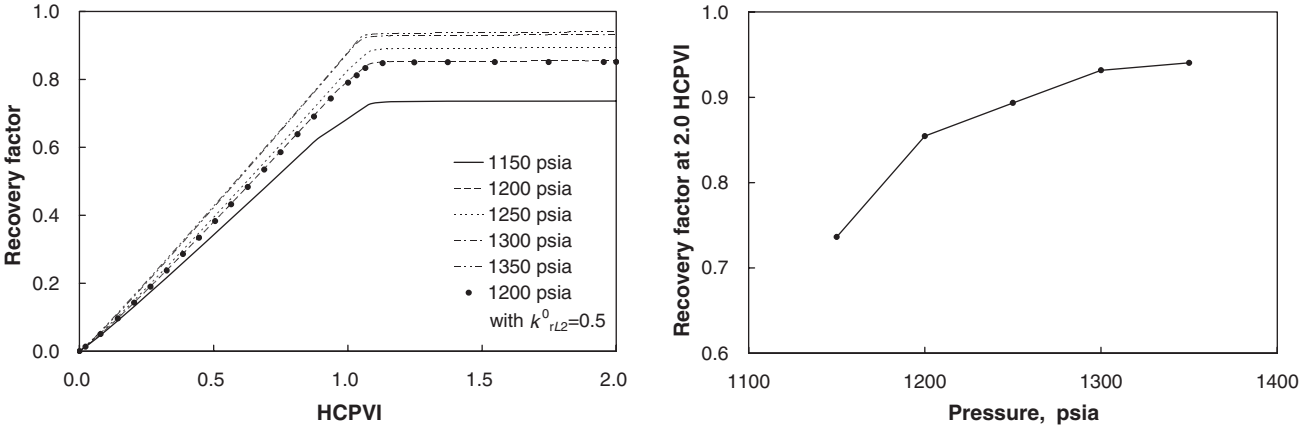

Fig. 25—Left: Oil recoveries for the displacements of the BSB oil at 105°F at different pressures by the injection gas given in Table 1. k^0_{rL2} is the endpoint relative permeability for the L_2 phase. Right: Oil recoveries at 2.0 HCPVI for the displacements shown on the left.

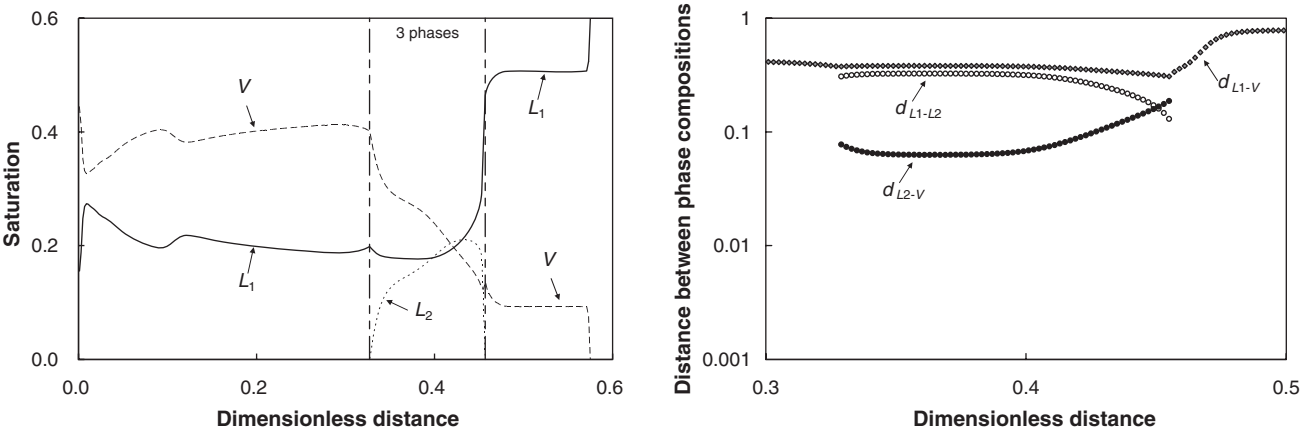

Fig. 26—Left: Profiles of phase saturations at 0.5 HCPVI for the BSB oil displacement at 105°F and 1,150 psia by the injection gas given in Table 1. Right: Distances between phase compositions in composition space at 0.5 HCPVI for the BSB oil displacement at 105°F and 1,150 psia by the injection gas given in Table 1.

Downloaded from http://onepetro.org/SJ/article-pdf/16/04/751/2106980/spe-129846-pa.pdf/1 by The University of Texas At Austin user on 18 September 2022

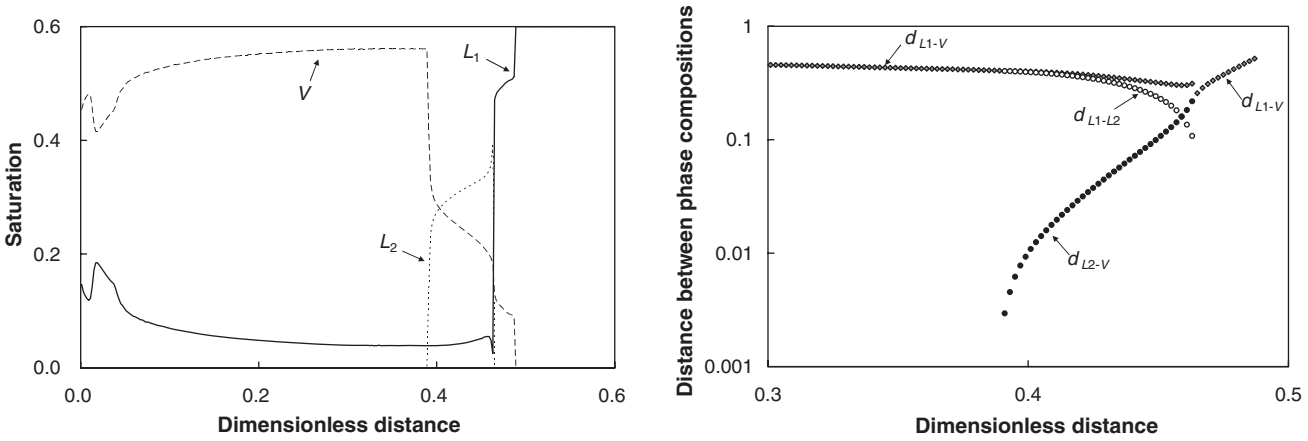

Fig. 27—Left: Profiles of phase saturations at 0.5 HCPVI for the BSB oil displacement at 105°F and 1,300 psia by the injection gas given in Table 1. Right: Distances between phase compositions in composition space at 0.5 HCPVI for the BSB oil displacement at 105°F and 1,300 psia by the injection gas given in Table 1.

simulation. As for the quaternary displacements, the L_1-V two-phase regions exist ahead of and behind the L_1-L_2-V three-phase region. The gas bank at the displacement front does not efficiently displace the oil, leaving the high L_1 phase saturation behind it. As pressure increases, the three-phase region becomes narrower and the L_2 phase saturation increases in the three-phase region. The sharp reduction in the L_1 phase saturation and increase in the L_2 phase saturation at the front of the three-phase region indicate the efficient extraction of components in the oil by the L_2 phase. The extraction becomes more significant as pressure increases, resulting in greater oil recovery.

Fig. 26 shows the equilibrium-phase composition distances at 0.5 HCPVI for the displacement at 1,150 psia. A similar plot is given in Fig. 27 for 1,300 psia. The compositional distance $d_{L2\text{-}V}$ exhibits a significant sensitivity to displacement pressure. At 1,150 psia, the L_2 phase is highly immiscible with the V phase in the three-phase region although $d_{L2\text{-}V}$ is smaller than $d_{L1\text{-}L2}$ and $d_{L1\text{-}V}$ except near the front of the three-phase region. At 1,300 psia, $d_{L2\text{-}V}$ asymptotically decreases at the tail of the three-phase region, indicating a near-critical state between the L_2 and V phases. However, as $d_{L1\text{-}L2}$ indicates, another coexisting phase L_1 is immiscible with the L_2 and V phases at the tail of the three-phase region. $d_{L1\text{-}L2}$ is smaller at the front of the three-phase region compared with other points in the three-phase region. The V phase is immiscible with the coexisting L_1 and L_2 phases at the front of the three-phase region, as shown by $d_{L1\text{-}V}$.

In the BSB oil displacements, the high displacement efficiency is achieved when the composition path goes near the UCEP tie line and, to a lesser extent, the LCEP tie line, as indicated in Fig. 27. When the composition path goes near the LCEP tie line at the front of the three-phase region, mass transfer between the L_2 and L_1 phases becomes significant because of near-miscibility between the two phases. When disappearing at the tail of the three-phase region, the L_2 phase efficiently merges into the V phase near the LCEP. As before, oil components are transferred from the L_1 to the V phase using the L_2 phase as a buffer.

In the simulations thus far, the V and L_2 phases had the same relative permeability curves as shown in Table 3. To examine the effect of L_2-phase relative permeability on the BSB oil displacement, the BSB oil displacements at 1,200 and 1,300 psia are repeated, assuming that the L_1 and L_2 phases have the same end-point relative permeability value of 0.50. Fig. 25 shows that this change in relative permeability results in only a marginal effect on the BSB oil displacement efficiency at 1,200 psia.

Conclusions

We presented the first detailed study of the complex three-phase behavior that occurs during low-temperature oil displacements by CO_2 solvent. We used a compositional simulator capable of robust three-phase equilibrium calculations to derive the mechanism for high displacement efficiency. The effects of three-phase behavior on displacement efficiency were systematically investigated using four-component EOS fluid models with varying pressure, temperature, and oil-component properties. The quaternary representation enabled us to visualize the complex three-phase behavior associated with CEP tie lines. A case study using a west Texas oil confirmed that the mechanism derived using quaternary fluids also holds for a reservoir oil model with seven components. The conclusions are as follows:

1. High efficiency of low-temperature oil displacements by CO_2 solvent occurs when the composition path traverses near the UCEP tie line and, to a lesser extent, the LCEP tie line. The LCEP at the front of the three-phase region results in efficient extraction of oil components by the L_2 phase. The L_2 phase merges into the V phase when it disappears at the tail of the three-phase region near the UCEP tie line. This efficient transfer of the components in the L_2 phase associated with near-UCEP behavior results in low L_1-phase saturation in the swept zone (i.e., high displacement efficiency). That is, the L_2 phase serves as a buffer between the immiscible V and L_1 phases within the three-phase region.
2. In the displacements studied, high displacement efficiency is a consequence of both condensation and vaporization of intermediate components. The L-V two-phase regions ahead of and behind the three-phase region exhibit condensation and vaporization behavior, respectively. Within the three-phase region, condensation and vaporization of intermediate components occur simultaneously because of the two CEPs, UCEP and LCEP.
3. As predicted by the phase rule for critical points, at least four components must be used for the EOS fluid model to develop CEPs in composition space at a fixed temperature and pressure. The quaternary representation provides qualitatively correct characteristics of low-temperature oil displacements by CO_2 solvent.
4. Nearly piston-like displacement is achieved because of the CEP behavior. Complete miscibility at a tricritical point is not necessary for the oil displacements studied in this paper.
5. Reservoir temperature and the composition of the oil can significantly affect the efficiency of low-temperature oil displacements by CO_2. The displacement efficiency is higher at lower reservoir temperature or for a lighter oil.
6. The three-phase region is typically larger than is indicated by a P–x diagram between reservoir oil and injection gas. Thus, the lower bound of pressure for the three-phase region on a P–x diagram is not a reliable indicator of the MMP.
7. The dissimilarity parameter defined in this paper increases as immiscibility between the three equilibrium phases increases for the fluids studied in this paper. Higher pressure is required to achieve the same displacement efficiency at a fixed temperature for a larger value of the dissimilarity parameter.

Downloaded from http://onepetro.org/SJ/article-pdf/16/04/751/2106980/spe-129846-pa.pdf/1 by The University of Texas At Austin user on 18 September 2022

Nomenclature

a = attraction parameter
b = covolume parameter
C = carbon number
d = distance in composition space defined in Eq. 1
g = parameter for the reduced method
h = parameter for the reduced method
K = K-value
L_1 = oleic phase
L_2 = CO_2-rich liquid phase
MW = molecular weight
N_c = number of components
P = pressure
T = temperature
V = gaseous phase or molar volume
x_{ij} = mole fraction of component i in phase j
ξ = dimensionless parameter defined in Eq. 2

Subscripts

C = critical value or component
i = component index
j = phase index
m = mixture

Acknowledgments

We thank the Japan Petroleum Exploration Company and the Japan Oil, Gas and Metals National Corporation for support of this research, along with the member companies of the gasflooding joint-industry project at the University of Texas at Austin, which is now located at the Pennsylvania State University.

References

Alwani, Z. and Schneider, G.M. 1976. Fluid Mixtures at High Pressure. Phase Separation and Critical Phenomena in Binary Mixtures of a Polar Component With Supercritical Carbon Dioxide, Ethane, and Ethene up to 1000 Bar. *Berichte der Bunsengesellschaft fuer Physikalische Chemie* **80** (12): 1310–1315.

Chaback, J.J. and Turek, E.A. 1986. Phase Behavior of Mixtures of San Andres Formation Oils With Acid Gases. Application of a Modified Redlich-Kwong Equation of State. In *Equations of State Theories and Applications*, ed. K.-C. Chao and R.L. Robinson Jr., Chap. 20, 406–433. Washington, DC: Symposium Series, ACS.

Chang, Y.-B., Pope, G.A., and Sepehrnoori, K. 1990. A higher-order finite-difference compositional simulator. *J. Pet. Sci. Eng.* **5** (1): 35–50. doi: 10.1016/0920-4105(90)90004-M.

Coutinho, J.A.P., Jørgensen, M., and Stenby, E.H. 1995. Predictions of three-phase regions in CO_2-oil mixtures. *J. Pet. Sci. Eng.* **12** (3): 201–208. doi: 10.1016/0920-4105(94)00044-5.

Creek, J.L. and Sheffield, J.M. 1993. Phase Behavior, Fluid Properties, and Displacement Characteristics of Permian Basin Reservoir Fluid/CO_2 Systems. *SPE Res Eng* **8** (1): 34–42. SPE-20188-PA. doi: 10.2118/20188-PA.

Davenport, A.J. and Rowlinson, J.S. 1963. The solubility of hydrocarbons in liquid methane. *Transactions of the Faraday Society* **59:** 78–84. doi: 10.1039/tf9635900078.

Davenport, A.J., Rowlinson, J.S., and Saville, G. 1966. Solutions of three hydrocarbons in liquid methane. *Transactions of the Faraday Society* **62:** 322–327. doi: 10.1039/tf9666200322.

Deiters, U. and Schneider, G.M. 1976. Fluid Mixtures at High Pressures. Computer Calculations of the Phase Equilibria and the Critical Phenomena in Fluid Binary Mixtures From the Redlich-Kwong Equation of State. *Berichte der Bunsengesellschaft fuer Physikalische Chemie* **80** (12): 1316–1321.

Deiters, U.K. and Pegg, I.L. 1989. Systematic investigation of the phase behavior in binary fluid mixtures. I. Calculations based on the Redlich–Kwong equation of state. *J. Chem. Phys.* **90** (11): 6632–6641. doi: 10.1063/1.456280.

Enick, R., Holder, G.D., and Morsi, B.I. 1985. Critical and three phase behavior in the carbon dioxide/tridecane system. *Fluid Phase Equilibria* **22** (2): 209–224. doi: 10.1016/0378-3812(85)85020-2.

Galindo, A. and Blas, F.J. 2002. Theoretical Examination of the Global Fluid Phase Behavior and Critical Phenomena in Carbon Dioxide + *n*-Alkane Binary Mixtures. *J. Phys. Chem. B* **106** (17): 4343–4564. doi: 10.1021/jp013402h.

Gardner, J.W., Orr, F.M. Jr., and Patel, P.D. 1981. The Effect of Phase Behavior on CO_2-Flood Displacement Efficiency. *J Pet Technol* **33** (11): 2067–2081. SPE-8367-PA. doi: 10.2118/8367-PA.

Gauter, K. 1999. Fluid Multiphase Behavior in Ternary Systems of Near-Critical CO_2. PhD dissertation, Technische Universität Berlin (TUB), Berlin, Germany.

Gauter, K., Heidemann, R.A., and Peters, C.J. 1999. Modeling of Fluid Multiphase Equilibria in Ternary Systems of Carbon Dioxide as the Near-Critical Solvent and Two Low-Volatile Solutes. *Fluid Phase Equilibria* **158–160** (June): 133–141. doi: 10.1016/S0378-3812(99)00122-3.

Gregorowicz, J. and de Loos, Th.W. 1996. Modelling of the three phase LLV region for ternary hydrocarbon mixtures with the Soave-Redlich-Kwong equation of state. *Fluid Phase Equilibria* **118** (1): 121–132. doi: 10.1016/0378-3812(95)02845-5.

Henry, R.L. and Metcalfe, R.S. 1983. Multiple-Phase Generation During Carbon Dioxide Flooding. *SPE J.* **23** (4): 595–601. SPE-8812-PA. doi: 10.2118/8812-PA.

Holm, L.W. and Josendal, V.A. 1974. Mechanisms of Oil Displacement By Carbon Dioxide. *J Pet Technol* **26** (12): 1427–1438. SPE-4736-PA. doi: 10.2118/4736-PA.

Holm, L.W. and Josendal, V.A. 1980. Discussion of Determination and Prediction of CO_2 Minimum Miscibility Pressures. *J Pet Technol* **32** (1):160–168. SPE-8876-DS. doi: 10.2118/7477-PA.

Holm, L.W. and Josendal, V.A. 1982. Effect of Oil Composition on Miscible-Type Displacement by Carbon Dioxide. *SPE J.* **22** (1): 87–98. SPE-8814-PA. doi: 10.2118/8814-PA.

Huang, E.T.S. and Tracht, J.H. 1974. The Displacement of Residual Oil by Carbon Dioxide. Paper SPE 4735 presented at the SPE Improved Oil Recovery Symposium, Tulsa, 22–24 April. doi: 10.2118/4735-MS.

Huie, N.C. 1972. The Heterogeneous Phase Equilibria of Carbon Dioxide-Normal Paraffin Systems. PhD dissertation, University of Notre Dame, Notre Dame, Indiana.

Johns, R.T. and Orr, F.M. Jr. 1996. Miscible Gas Displacement of Multicomponent Oils. *SPE J.* **1** (1): 39–50. SPE-30798-PA. doi: 10.2118/30798-PA.

Katz, D.L. and Firoozabadi, A. 1978. Predicting Phase Behavior of Condensate/Crude-Oil Systems Using Methane Interaction Coefficients. *J Pet Technol* **30** (11): 1649–1655. SPE-6721-PA. doi: 10.2118/6721-PA.

Khan, S.A. 1992. An Expert System to Aid in Compositional Simulation of Miscible Gas Flooding. PhD dissertation. 1992. PhD dissertation, University of Texas at Austin, Austin, Texas (December 1992).

Khan, S.A., Pope, G.A., and Sepehrnoori, K. 1992. Fluid Characterization of Three-Phase CO_2/Oil Mixtures. Paper SPE 24130 presented at the SPE/DOE Enhanced Oil Recovery Symposium, Tulsa, 22–24 April. doi: 10.2118/24130-MS.

Kohn, J.P., Kim, Y.J., and Pan, Y.C. 1966. Partial Miscibility Phenomena in Binary Hydrocarbon Systems Involving Ethane. *J. Chem. Eng. Data* **11** (3): 333–335. doi: 10.1021/je60030a012.

LaForce, T. 2005. Mathematics of Partially Miscible Three-Phase Flow. PhD dissertation. 2005. PhD dissertation, University of Texas, Austin, Texas (May 2005).

LaForce, T. and Johns, R.T. 2005. Composition Routes for Three-Phase Partially Miscible Flow in Ternary Systems. *SPE J.* **10** (2): 161–174. SPE-89438-PA. doi: 10.2118/89438-PA.

Larson, L.L., Silva, M.K., Taylor, M.A., and Orr, F.M. Jr. 1989. Temperature Dependence of $L_1/L_2/V$ Phase Behavior in CO_2/Hydrocarbon Systems. *SPE Res Eng* **4** (1): 105–114. SPE-15399-PA. doi: 10.2118/15399-PA.

Larson, R.G. 1979. The Influence of Phase Behavior on Surfactant Flooding. *SPE J.* **19** (6): 411–422. SPE-6774-PA. doi: 10.2118/6774-PA.

Lim, M.T., Khan, S.A., Sepehrnoori, K., and Pope, G.A. 1992. Simulation of Carbon Dioxide Flooding Using Horizontal Wells. Paper SPE 24929 presented at the SPE Annual Technical Conference and Exhibition, Washington, DC, 4–7 October. doi: 10.2118/24929-PA.

Metcalfe, R.S. and Yarborough, L. 1979. The Effect of Phase Equilibria on the CO_2 Displacement Mechanism. *SPE J.* **19** (4): 242–252; *Trans.,* AIME, **267.** SPE-7061-PA. doi: 10.2118/7061-PA.

Downloaded from http://onepetro.org/SJ/article-pdf/16/04/751/2106980/spe-129846-pa.pdf/1 by The University of Texas At Austin user on 18 September 2022

Miller, M.M. and Luks, K.D. 1989. Observations on the multiphase equilibria behavior of CO_2-rich and ethane-rich mixtures. *Fluid Phase Equilibria* **44** (3): 295–304. doi: 10.1016/0378-3812(89)80059-7.

Mushrif, S.H. 2004. Determining Equation of State Binary Interaction Parameters Using K- and L-Points. MS thesis, University of Saskatchewan, Saskatoon, Canada (October 2004).

Mushrif, S.H. and Phoenix, A.V. 2008. Effect of Peng-Robinson Binary Interaction Parameters on the Predicted Multiphase Behavior of Selected Binary Systems. *Ind. Eng. Chem. Res.* **47** (16): 6280–6288. doi: 10.1021/ie800599t.

Okuno, R. 2009. Modeling of Multiphase Behavior for Gas Flooding Simulation. PhD dissertation. 2009. PhD dissertation, University of Texas at Austin, Austin, Texas (August 2009).

Okuno, R., Johns, R.T., and Sepehrnoori, K. 2010c. Three-Phase Flash in Compositional Simulation Using a Reduced Method. *SPE J.* **15** (3): 689–703. SPE-125226-PA. doi: 10.2118/125226-PA.

Okuno, R., Johns, R.T., and Sepehrnoori, K. 2010a. A New Algorithm for Rachford-Rice for Multiphase Compositional Simulation. *SPE J.* **15** (2): 313–325. SPE-117752-PA. doi: 10.2118/117752-PA.

Okuno, R., Johns, R.T., and Sepehrnoori, K. 2010b. Application of a Reduced Method in Compositional Simulation. *SPE J.* **15** (1): 39–49. SPE-119657-PA. doi: 10.2118/119657-PA.

Orr, F.M. Jr. 2007. *Theory of Gas Injection Processes*. Copenhagen, Denmark: Tie-Line Publications.

Orr, F.M. Jr. and Jensen, C.M. 1984. Interpretation of Pressure-Composition Phase Diagrams for CO_2/Crude Oil Systems. *SPE J.* **24** (5): 485–497. SPE-11125-PA. doi: 10.2118/11125-PA.

Orr, F.M. Jr., Silva, M.K., and Lien, C.-L. 1983. Equilibrium Phase Compositions of CO_2/Crude Oil Mixtures-Part 2: Comparison of Continuous Multiple-Contact and Slim-Tube Displacement Tests. *SPE J.* **23** (2): 281–291. SPE-10725-PA. doi: 10.2118/10725-PA.

Orr, F.M. Jr., Yu, A.D., and Lien, C.L. 1981. Phase Behavior of CO_2 and Crude Oil in Low-Temperature Reservoirs. *SPE J.* **21** (4): 480–492. SPE-8813-PA. doi: 10.2118/8813-PA.

Pedersen, K.S. and Christensen, P.L. 2007. *Phase Behavior of Petroleum Reservoir Fluids*. Boca Raton, Florida, USA: CRC Press.

Pedersen, K.S., Blilie, A.L., and Meisingset, K.K. 1992. PVT calculations on petroleum reservoir fluids using measured and estimated compositional data for the plus fraction. *Ind. Eng. Chem. Res.* **31** (5): 1378–1384. doi: 10.1021/ie00005a019.

Pedersen, K.S., Milter, J., and Sørensen, H. 2004. Cubic Equations of State Applied to HT/HP and Highly Aromatic Fluids. *SPE J.* **9** (2): 186–192. SPE-88364-PA. doi: 10.2118/88364-PA.

Pedersen, K.S., Rasmussen, P., and Fredenslund, A. 1985. Thermodynamics of petroleum mixtures containing heavy hydrocarbons. 3. Efficient flash calculation procedures using the SRK equation of state. *Ind. Eng. Chem. Process Des. Dev.* **24** (4): 948–954. doi: 10.1021/i200031a009.

Pedersen, K.S., Thomassen, P., and Fredenslund, A. 1984b. Thermodynamics of petroleum mixtures containing heavy hydrocarbons. 2. Flash and PVT calculations with the SRK equation of state. *Ind. Eng. Chem. Process Des. Dev.* **23** (3): 566–573. doi: 10.1021/i200026a027.

Pedersen, K.S., Thomassen, P., and Fredenslund, A.A. 1984a. Thermodynamics of petroleum mixtures containing heavy hydrocarbons. 1. Phase envelope calculations by use of the Soave-Redlich-Kwong equation of state. *Ind. and Eng. Chem. Proc. Des. Dev.* **23** (1): 163–170. doi: 10.1021/i200024a027.

Peng, D.-Y. and Robinson, D.B. 1976. A New Two-Constant Equation of State. *Ind. Eng. Chem. Fundamentals* **15** (1): 59–64. doi: 10.1021/160057a011.

Riazi, M.R. and Daubert, T.E. 1980. Simplify Property Predictions. *Hydrocarb. Process.* **59** (3): 115–116.

Rowlinson, J.S. and Freeman, P.I. 1961. Lower critical solution points in hydrocarbon mixtures. *Pure and Applied Chemistry* **2** (1–2): 329–334. doi: 10.1351/pac196102010329.

Scott, R.L. and van Konynenburg, P.H. 1970. Static properties of solutions. Van der Waals and related models for hydrocarbon mixtures. *Discussions of the Faraday Society* **49:** 87–97. doi: 10.1039/df9704900087.

Shelton, J.L. and Yarborough, L. 1977. Multiple Phase Behavior in Porous Media During CO_2 or Rich-Gas Flooding. *J Pet Technol* **29** (9): 1171–1178. SPE-5827-PA. doi: 10.2118/5827-PA.

Stalkup, F.I. 1978. Carbon Dioxide Miscible Flooding: Past, Present, and Outlook for the Future. *J Pet Technol* **30** (8): 1102–1112. SPE-7042-PA. doi: 10.2118/7042-PA.

Stewart, W.C. and Nielsen, R.F. 1953. Phase Equilibria for Mixtures of Carbon Dioxide and Several Normal Saturated Hydrocarbons. Engineering Experiment Station Bulletin No. 62, Pennsylvania State College, State College, Pennsylvania, 19–29.

Turek, E.A., Metcalfe, R.S., and Fishback, R.E. 1988. Phase Behavior of Several CO_2/West Texas-Reservoir-Oil Systems. *SPE Res Eng* **3** (2): 505–516. SPE-13117-PA. doi: 10.2118/13117-PA.

Uzunov, D.I. 1993. *Introduction to the Theory of Critical Phenomena*. Singapore: World Scientific Publishing.

van Konynenburg, P.H. 1968. Critical Lines and Phase Equilibria in Binary Mixtures. PhD dissertation, University of California, Los Angeles, California.

Van Konynenburg, P.H. and Scott, R.L. 1980. Critical Lines and Phase Equilibria in Binary van der Waals Mixtures. *Phil. Trans. R. Soc. Lond. A* **298** (1442): 495–540. doi: 10.1098/rsta.1980.0266.

Wagner, J.R., McCaffrey, D.S., and Kohn, J.P. 1968. Partial miscibility phenomena in the ternary system ethane-n-hexadecane-n-eicosane. *J. Chem. Eng. Data* **13** (1): 22–24. doi: 10.1021/je60036a007.

Yang, Q. 2006. Automatic Development of Global Phase Diagrams for Binary Systems in Pressure-Temperature Space. MS thesis, University of Saskatchewan, Saskatoon, Canada (August 2006).

Yellig, W.F. and Metcalfe, R.S. 1980. Determination and Prediction of CO_2 Minimum Miscibility Pressures. *J Pet Technol* **32** (1): 160–168. SPE-7477-PA. doi: 10.2118/7477-PA.

Yuan, H., Johns, R.T., Egwuenu, A.M., and Dindoruk, B. 2005. Improved MMP Correlation for CO_2 Floods Using Analytical Gas Flooding Theory. *SPE Res Eval & Eng* **8** (5): 418–425. SPE-89359-PA. doi: 10.2118/89359-PA. See also Errata, *SPE Res Eval & Eng* **9** (4).

SI Metric Conversion Factors

ft × 3.048	E–01 = m
°F (°F -32)/1.8	= °C
lbm × 4.535 924	E–01 = kg
psi × 6.894 757	E+00 = kPa

Ryosuke Okuno is an Assistant Professor of Petroleum Engineering in the Department of Civil and Environmental Engineering at the University of Alberta. He has 7 years of industrial experience as a reservoir engineer with the Japan Petroleum Exploration Company. His research interests include modeling of multiphase behavior, enhanced oil recovery, and thermal oil recovery. Okuno holds BS and MS degrees in geosystem engineering from the University of Tokyo and a PhD degree in petroleum engineering from the University of Texas at Austin. **Russell T. Johns** holds the Victor and Anna Mae Beghini Faculty Fellowship in Petroleum and Natural Gas Engineering at the Pennsylvania State University at University Park. His research interests include theory of gas-injection processes, multiphase flow in porous media, and well testing. Johns holds a BS degree in electrical engineering from Northwestern University and MS and PhD degrees in petroleum engineering from Stanford University. **Kamy Sepehrnoori** is the Bank of America Professor in the Department of Petroleum and Geosystems Engineering at the University of Texas at Austin. His research and teaching interests include computational methods, reservoir simulation, parallel computations, enhanced-oil-recovery modeling, and inverse modeling. He holds a PhD degree from the University of Texas at Austin.

Downloaded from http://onepetro.org/SJ/article-pdf/16/04/751/2106980/spe-129846-pa.pdf/1 by The University of Texas At Austin user on 18 September 2022